Functional characterization of the thrombospondin-related paralogous proteins rhoptry discharge factor 1 and 2 unveils phenotypic plasticity in *Toxoplasma gondii* rhoptry exocytosis

Alessia Possenti[1¶], Manlio Di Cristina[2¶], Chiara Nicastro[1], Matteo Lunghi[2,3], Valeria Messina[1], Federica Piro[2], Lorenzo Tramontana[1], Simona Cherchi[1], Mario Falchi[1], Lucia Bertuccini[1], Furio Spano[1]*

[1]Department of Infectious Diseases, Istituto Superiore di Sanità, Rome, Italy

[2]Department of Chemistry, Biology and Biotechnology, University of Perugia, Perugia, Italy

[#a]Current address: Department of Microbiology and Molecular Medicine, University of Geneva, CMU, Geneva, Switzerland

*Corresponding author

E-mail: furio.spano@iss.it

[¶]These authors contributed equally to this work

Abstract

To gain access to the intracellular cytoplasmic niche essential for their growth and replication, apicomplexan parasites such as *Toxoplasma gondii* rely on the timely secretion of two types of apical organelles named micronemes and rhoptries. Rhoptry proteins are key to host cell invasion and remodelling, however, the molecular mechanisms underlying the thight control of rhoptry discharge are poorly understood. Here, we report the identification and functional characterization of two novel *T. gondii* thrombospondin-related proteins implicated in rhoptry exocytosis. The two proteins, already annotated as MIC15 and MIC14, were renamed rhoptry discharge factor 1 (RDF1) and rhoptry discharge factor 2 (RDF2) and found to be exclusive of the Coccidia class of apicomplexan parasites. Furthermore, they were shown to have a paralogous relationship and share a C-terminal transmembrane domain followed by a short cytoplasmic tail. Immunofluorescence analysis of *T. gondii* tachyzoites revealed that RDF1 presents a diffuse cytoplasmic localization not reminiscent of any know subcellular compartment, whereas RDF2 was not detected. Using a conditional knockout approach, we demonstrated that RDF1 loss caused a marked growth defect. The lack of the protein did not affect parasite gliding motility, host cell attachment, replication and egress, whereas invasion was dramatically reduced. Notably, while RDF1 depletion did not result in altered microneme exocytosis, rhoptry discharge was found to be heavily impaired. Interestingly, rhoptry secretion was partially reversed by spontaneous upregulation of the *RDF2* gene in knockdown parasites grown under constant *RDF1* repression. Collectively, our results identify RDF1 and RDF2 as additional key players in the pathway controlling rhoptry discharge. Furthermore, this study unveils a new example of compensatory mechanism contributing to phenotypic plasticity in *T. gondii.*

Author Summary

The Apicomplexa include obligate intracellular parasites posing a serious threath to human health, such as the malaria-causing *Plasmodium* spp., and the opportunistic *Toxoplasma gondii*

responsible for severe birth defects if congenitally transmitted. These organisms possess an apical complex, comprising tubulin-based structures and secretory organelles named micronemes and rhoptries. The release of micronemal adhesins is instrumental to parasite gliding motility, host cell attachment and invasion and precedes rhoptry discharge. At the onset of invasion, released rhoptry neck proteins lead to the formation of the moving junction, a ring-like structure through which the parasite invades the host cell, then rhoptry bulb proteins injected into the host cell contribute to parasitophorous vacuole formation and host cell subversion. While the signals underlying microneme secretion have been significantly elucidated, the understanding of the mechanisms governing rhoptry secretion is still in its infancy. We have identified two thrombospondin-related paralogous proteins of *T. gondii*, RDF1 and RDF2, playing a key role in this process. Conditional depletion of RDF1 dramatically impacts rhoptry exocytosis and invasion. Furthermore, in RDF1 depleted parasites the rhoptry secretion defect is partially rescued by the transcriptional upregulation of *RDF2*. These results shed further light on the molecular players involved in rhoptry discharge and unveil a new example of *T. gondii* phenotypic plasticity.

Introduction

The protozoan *Toxoplasma gondii* is an obligate intracellular parasite of the phylum Apicomplexa, which includes several other pathogens belonging to genera of great medical or veterinary relevance such as *Plasmodium*, *Cryptosporidium*, *Eimeria* and *Theileria*. Toxoplasmosis affects humans and farm animals worldwide, causing life-threatening infections in immunocompromised subjects, and abortion or serious birth defects if congenitally transmitted to the fetus. Seroprevalence data indicate that one third of the human population has been exposed to *T. gondii* and is likely chronically infected.

The symptomatic manifestations of acute toxoplasmosis depend on tachyzoites, which

76 couple efficient dissemination to any body district of the infected host to a fast replicating
77 phenotype, leading to tissue damage. Before the onset of the host immune response, *T. gondii*
78 tachyzoites undergo multiple lytic cycles marked by four sequential steps, i.e., host cell
79 attachment, active invasion, intravacuolar replication and lytic egress. During the motile phases of
80 the lytic cycle, a major role is played by the apical complex, a sophisticated system of cytoskeletal
81 and vesicular elements distinctive of the invasive stages of Apicomplexa. The cytoskeletal
82 component includes the conoid, a peculiar structure made of spirally arranged tubulin fibers that
83 is reversibly extruded during parasite gliding motility, invasion and egress [1]. Membrane bound
84 elements include an array of non secretory apical vesicles [2,3] and two types of secretory
85 organelles, called micronemes and rhoptries, that discharge their content in a sequential and
86 tightly regulated fashion, orchestrating the transition from the extracellular to the intravacuolar
87 environment. Upon microneme secretion [4], various transmembrane adhesins are apically
88 exposed on the parasite plasma membrane (PM) and act as a link between extracellular ligands
89 and the subpellicular acto-myosin motor of the parasite, playing a key role in substrate-dependent
90 gliding motility, host cell attachment and invasion. The club-shaped rhoptries consist of an
91 elongated neck passing through the conoid and a posterior bulb [5]. These two organellar districts
92 contain specific sets of proteins called RONs and ROPs, respectively, which are released from the
93 rhoptries upon host cell attachment and microneme secretion. When a complex of specific RON
94 proteins is inserted into the host cell membrane and recognized by the micronemal protein apical
95 membrane antigen-1 (AMA1) displayed on the tachyzoite surface, a ring-like moving junction is
96 produced [6,7], that allows parasite firm attachment to and traversal of the host cell PM.
97 Following RONs secretion, ROP proteins are injected into the host cell cytoplasm within clusters of
98 small vesicles called evacuoles [8] and contribute to parasitophorous vacuole formation,
99 modulation of host cell transcription and virulence [5].

100 In the complex interplay between *T. gondii* and the host cell, a prominent role is played by
101 modular proteins containing adhesive amino acid motifs conserved in metazoan organisms, such
102 as the PAN/Apple, epidermal growth factor-like, von Willebrand factor type A (vWA) and
103 thrombospondin type 1 (TSP1) domains. This latter motif of approximately 60 amino acids is able
104 to bind carbohydrate and protein substrates and was identified in the extracellular matrix
105 glycoprotein thrombospondin-1 and in dozens of other human proteins involved in cell-to-cell an
106 cell-to-matrix interactions [9]. In apicomplexan parasites the TSP1 domain is present in several
107 secretory proteins fulfilling important functions. In *Plasmodium* spp., stage-specific members of
108 the TSP1 domain superfamily are implicated in processes as diverse as gliding motility, cell binding,
109 invasion, egress and cell traversal and include the proteins CSP [10], TRAP [11], CTRP [12], MTRAP
110 [13], PTRAMP [14], TLP [15], TREP [16] and TRP1 [17]. Notably, except the surface GPI-anchored
111 CSP, all these proteins have a type I transmembrane (TM) topology and share with the prototypic
112 TRAP an extracellular adhesive domain, a C-terminal TM region and a cytoplasmic tail that
113 interacts with the force-generating acto-myosin system of the parasite. In *T. gondii*, MIC2 [18],
114 MIC12 [19] and MIC16 [20] are the only TSP1 domain-containing proteins characterized so far.
115 They share with *Plasmodium* members of the TRAP family the overall structural organization and
116 the localization to the micronemes. The most extensively characterized is the TRAP functional
117 ortholog MIC2, which plays a crucial role in tachyzoite host cell attachment [21] and is involved in
118 gliding motility and host cell egress [22]. MIC2 contains a single vWA domain and six tandemly
119 arrayed TSP1 motifs, one of which directly mediates the formation of a complex with the soluble
120 MIC2-associated protein (M2AP) essential for microneme targeting [23].

121 In the present work we explored the genome of *T. gondii* to search for additional and
122 functionally relevant proteins containing the TSP1 domain. We identified nine new members of
123 this protein subclass, the majority of which are expected to play important or essential roles based

124 on a genome wide CRISPR-Cas9 dataset [24]. We report herein on the functional characterization
125 of two paralogous TSP1 domain-containing proteins specific of Coccidia. Despite their TRAP-like
126 structural organization, the two proteins do not traffic to the micronemes but present a dispersed
127 cytoplasmic localization resembling that of proteins recently implicated in rhoptry secretion [2,25].
128 Using reverse genetics, we demonstrate that the two proteins represent novel rhoptry discharge
129 factors and that their redundancy confers to the parasite a further degree of phenotypic plasticity
130 capable to preserve an essential function related to host cell invasion.
131

132 Results

133 Definition of the repertoire of thrombospondin-related proteins in 134 *Toxoplasma gondii*

135 To expand our knowledge of the repertoire of TSP1 domain-containing proteins encoded by the *T.*
136 *gondii* genome, we searched the ToxoDB database with the PSI-BLAST algorithm using as query
137 the amino acid consensus sequence WXXWXXCXXXC spanning highly conserved amino acid
138 positions within the TSP1 domain. This allowed us to identify nine additional polypeptides
139 containing one or more copies of this amino acid motif. Table 1 summarizes the main
140 characteristics of the predicted proteins, including their major structural features, the expression
141 in different invasive stages and the fitness-conferring score (FCS). This value, derived from a
142 genome-wide loss of function genetic screen [24], ranks individual *T. gondii* proteins based on
143 their indispensability during the tachyzoite lytic cycle in cultured human fibroblasts. Interestingly,
144 seven of the newly identified TSP-related proteins had FCSs ranging from -0.48 to -3.9, with higher
145 negative values indicating a higher degree of protein essentiality. With the exception of
146 TGME49_279420 and TGME49_319992, all the identified proteins possess a single C-terminal

147 transmembrane region (TMR), however, only TGME49_209060 and TGME49_247195 have a
148 putative N-terminal leader peptide for targeting to the secretory pathway. The lack of this amino
149 acid element in the other proteins is possibly due to inaccurate 5'-end predictions. Out of five TSP-
150 related genes lacking proteomic-based expression evidence of the encoded proteins in
151 tachyzoites, bradyzoites or sporozoites, four (*TGME49_223480, TGME49_237585,*
152 *TGME49_247970* and *TGME49_319992*) show transcriptional profiles compatible with expression
153 in *T. gondii* enteric stages. Instead, *TGME49_218310* exhibits no significant stage-specific
154 upregulation. Mass-spectrometry data support expression of the four remaining proteins in
155 tachyzoites and in three cases (TGME49_209060, TGME49_247195 and TGME49_279420) also in
156 bradyzoites and sporozoites.

157 The protein TGME49_247195, annotated in ToxoDB as MIC15, is characterized by a
158 markedly negative FCS (-3.31), indicative of an important functional role. The predicted 2924
159 amino acid long MIC15 consists of a N-terminal leader peptide, a large ectodomain spanning three
160 TSP1 motifs and a C-terminal TMR followed by a putative cytoplasmic tail. This overall architecture
161 closely resembles that of several type I transmembrane adhesins secreted by the micronemes, and
162 key to *T. gondii* gliding motility (MIC2) [22], rhoptry secretion (MIC8) [26] or moving junction
163 formation (AMA1) [6,7]. Furthermore, BLAST analysis showed that the 968 amino acid long
164 TGME49_218310 identified by our search and annotated in ToxoDB as MIC14, shares 27% identity
165 and 41% similarity with the C-terminal third of MIC15 and a comparable domain organization.
166 Based on the hypothesis that MIC15 might play an important role in parasite-host cell interaction
167 and that the leaderless MIC14 might represent an incompletely predicted and closely related
168 homolog, we decided to characterize the two proteins in more detail.

169

170

171 **Table 1. Uncharacterized thrombospondin-related proteins in *Toxoplasma gondii***
172

ToxoDB gene ID	Chr. n.	ToxoDB annotation	FCS[a]	#TSP1 domains	Other domains	LP	TMR	length	Proteomics[b]	Transcriptomics[c]
TGME49_223480	X	sushi domain-containing protein	-3.9	16	Sushi, NL	no	yes	4752	nd	EES
TGME49_247195	XII	Microneme protein MIC15	-3.31	3	H-type lectin	yes	yes	2909	T,S,B	T,S,B
TGME49_277910	XII	TSP1 domain-containing protein	-2.95	1	--	no	yes	1232	T	all stages
TGME49_279420	IX	Hypothetical protein	-1.96	1	--	no	no	1329	T,S,B	T,S,B
TGME49_209060	Ib	TSP1 domain-containing protein	-1.7	7	--	yes	yes	876	T,S,B	all stages
TGME49_247970	XII	Hypothetical protein	-0.96	2	--	yes	yes	1237	nd	EES
TGME49_319992	IV	Hypothetical protein	-0.48	1	--	no	no	223	nd	EES
TGME49_218310	XII	Microneme protein MIC14	0.28	3	--	no	yes	968	nd	all stages
TGME49_237585	X	Hypothetical protein	1.41	2	--	no	yes	1253	T*	EES

173 [a]FCS: fitness conferring score [24] indicating protein essentiality (highly negative values) or dispensability (positive values)
174 [b]Stages in which the protein was identified by mass-spectrometry according to proteomic studies reported in ToxoDB
175 [c]Stages with the relative highest abundance of gene transcript as deduced from ToxoDB data
176 *Weak single-peptide identification
177 Abbreviations: B, bradyzoite; EES, enteroepithelial stages; LP, leader peptide; nd, no data; NL, Notch domain; S, sporozoite; T, tachyzoite; TMR,
178 transmembrane region; vWA, von Willebrand factor type A domain
179

180 Structure of the *MIC14* and *MIC15* genomic loci

181 To verify the ToxoDB gene models of *MIC14* and *MIC15,* which lie about 1.6 Mb apart on
182 chromosome XII, we screened a *T. gondii* (strain RH) cDNA library using a PCR-based limiting
183 dilution method [27] and isolated two polyadenylated cDNAs consisting of 4259 bp for *MIC14* and
184 5656 bp for *MIC15* (Figs 1A and B). The *MIC14* cDNA fully accounted for the 17 exons gene model
185 displayed in ToxoDB, whereas the *MIC15* cDNA spanned only the 23 terminal exons of the
186 predicted genomic locus. Using gene-specific reverse primers designed in the 5' end of the newly
187 isolated cDNAs, we subjected total tachyzoite RNA to 5' RACE elongations. By this approach we
188 extended the *MIC15* transcript by approximately 3.8 Kb (Fig 1A), obtaining a combined full-length
189 cDNA sequence of 9473 bp that confirmed the 42 exons structure of the genomic locus and the
190 MIC15 amino acid sequence reported in ToxoDB. On the contrary, 5' RACE experiments yielded no
191 *MIC14*-specific elongation products. However, a BLASTP search of ToxoDB with the MIC15 amino

192 acid sequence as query provided indirect evidence that the *MIC14* transcript might extend
193 considerably upstream of the cDNA 5' end. In fact, MIC15 showed significant homology (25%
194 identity, 40% similarity) with the hypothetical protein TGME49_218340 encoded by the gene lying
195 immediately upstream of the equally oriented *MIC14* (Fig 1B). Interestingly, the 1187 amino acid
196 long TGME49_218340 aligned for its entire length with the two N-terminal thirds of MIC15,
197 strongly suggesting that *TGME49_218340* and *TGME49_218310* (*MIC14*) belong to the same
198 transcriptional unit. As represented in Fig 1B, this hypothesis was confirmed by RT-PCR
199 amplification of a 4.5 Kb product that spanned the entire *TGME49_218340* transcript and
200 overlapped with the cloned *MIC14* cDNA. Using poly-A^+ tachyzoite RNA, the resulting transcript
201 was further extended by 5' RACE, yielding a combined mRNA sequence of 7593 bp (GenBank
202 accession number AY089992.2) that encoded a putative N-terminal signal-anchor sequence, and
203 brought MIC14 length from 968 to 2344 amino acids. As shown in Fig 1C, the corresponding
204 genomic locus consists of 43 exons, 25 of which are perfectly conserved with respect to *MIC15*.
205 To further investigate transcription at the *MIC14* locus, we carried out a Northern blot
206 analysis of tachyzoite RNA using the probes P5' and P3' (Fig 1D), mapping at the two extremes of
207 the *MIC14* locus. While the 3' end probe recognized a single RNA species of approximately 4.5 Kb
208 compatible with the size of the cloned *MIC14* cDNA, the 5' end probe showed no hybridization,
209 suggesting that in *T. gondii* tachyzoites the *MIC14* locus is predominantly transcribed as a 5'-
210 truncated mRNA form of approximately 4.5 Kb while the full-length transcript is scarcely
211 represented.
212

213 Phylogenetic relationship and structural organization of MIC14 and 214 MIC15

215 BLASTP searches for MIC14 and MIC15 homologs in vEuPathDB (https://veupathdb.org/) and in

216 the NCBI non-redundant proteins database recovered highly homologous sequences exclusively
217 from the phylum Apicomplexa and in particular from the Coccidia class, that includes parasitic
218 genera of high veterinary relevance such as *Eimeria*, *Neospora* and *Sarcocystis*. As illustrated in Fig
219 2A, the comparison between the amino acid sequences of MIC14 and MIC15 homologs retrieved
220 from eight genera of Coccidia yielded a robust phylogenetic tree demonstrating that the two
221 proteins have a paralogous relationship.

222 Pairwise alignment between the full-length amino acid sequences of MIC14 and MIC15
223 showed an identity of 19% (44% similarity) and a comparable domain organization (Fig 2B). The C-
224 terminal halves of MIC14 and MIC15 are characterized by two and three TSP1 domains,
225 respectively, followed by a C-terminally located TMR and cytoplasmic tails of 97 and 180 amino
226 acids, respectively. Moreover, the N-terminal region of both proteins contains two tandemly
227 arrayed cysteine-rich repeats of approximately 300 amino acids. Nonetheless, the two paralogs
228 differ for the presence in MIC15 of a H-type lectin carbohydrate-binding domain conserved in the
229 majority of the Coccidia genera analyzed. In addition, while MIC15 is predicted to have a cleavable
230 N-terminal leader peptide, in MIC14 this element is replaced by a putative N-terminal signal-
231 anchor sequence. However, these structural features were not strictly conserved throughout
232 evolution, as both MIC14 and MIC15 orthologs exhibit either of the two types of N-terminal
233 signals. Noteworthy, about 82% (108) of the cysteine residues distributed throughout *T. gondii*
234 MIC14 and MIC15 are conserved (S1 Fig), strongly suggesting a common three-dimensional
235 folding.

236

237 Expression and immunolocalization of MIC15

238 The expression of MIC15 in *T. gondii* tachyzoites was investigated by Western blot using two
239 distinct rabbit polyclonal antibodies denominated MIC15Nt, recognizing a protein region spanning

240 the H-type lectin domain, and MIC15Ct, directed against the C-terminal portion of the ectodomain
241 (Fig 2B). In total tachyzoite lysates, both antisera specifically recognized a single protein band >260
242 kDa, compatible with the MIC15 predicted molecular mass of approximately 300 kDa (Fig 3A, left
243 panel). The same antibodies showed no reactivity with the excreted-secreted antigen (ESA)
244 fraction from ethanol-treated parasites (Fig 3A, right panel), questioning the possibility that MIC15
245 is a new member of the group of microneme transmembrane adhesins which are proteolytically
246 shed from the parasite surface upon secretion [20]. In the majority of cases, this process is driven
247 by a parasite rhomboid protease recognizing an intramembrane amino acid sequence which is
248 absent from the TMR of both MIC15 and MIC14 (S2 Fig).

249 The possible exposure of MIC15 on the parasite PM was investigated by indirect
250 immunofluorescence analysis (IFA) in non permeabilized tachyzoites of strain RH dual stained with
251 the MIC15Nt rabbit serum and an anti-SAG1 mAb as positive control. As shown in Fig 3B, the anti-
252 MIC15 antibodies showed no surface reactivity, whereas in detergent treated parasites they
253 produced a punctate diffuse cytoplasmic signal. This unexpected localization was then studied in
254 intravacuolar tachyzoites using the rabbit serum MIC15Nt in conjunction with antibodies to a
255 series of reference intracellular structures (Fig 3C). The staining pattern confirmed a diffuse dotted
256 distribution of the protein throughout the parasite cytoplasm and showed no MIC15 colocalization
257 with apical organelles, micronemes and rhoptries, or with dense granule proteins. This unexpected
258 result was independently supported by IFA of three distinct parasite lines in which MIC15 was
259 endogenously tagged by adding either the spaghetti monster-c-myc (smMYC) protein at the N-
260 terminus, a Ty epitope upstream of the TMR or two HA tags at the C-terminus. All endogenous
261 taggings were confirmed by Western blot analysis, showing that tagged strains expressed similar
262 MIC15 protein levels (S3 Figs A-C). All three mutants exhibited the same punctate staining pattern
263 irrespective of the tagging strategy adopted (Fig 3D and S3D Fig). Taken together, the

264 immunolocalization studies showed that MIC15 has a diffuse cytoplasmic distribution reminiscent
265 of that recently reported for a series of proteins essential for *T. gondii* rhoptry secretion, including
266 the calcium sensor TgFER2 [25] and members of the so-called "non-discharge" (Nd) protein family
267 conserved in the Alveolata superphylum [2].
268

269 Generation of a *MIC15* conditional knockout mutant

270 To gain functional insights into MIC15 function, we tried to disrupt the encoding gene by double
271 homologous recombination in the RHΔ*ku80 T. gondii* strain. Following repeated failures of this
272 approach supporting the predicted essentiality of MIC15, we generated an inducible knockdown
273 parasite line, named MIC15-iKD, in the TATiΔ*ku80* strain [28,29]. To this aim, we replaced the cell
274 cycle regulated promoter of *MIC15* with a constitutive, tetracycline-repressible regulatory element
275 (TRE), consisting of seven tandemly arrayed TetO sequences placed immediately upstream of the
276 SAG4 minimal promoter S4 (Fig 4A). Correct construct integration and endogenous promoter
277 replacement was confirmed by PCR (Fig 4B). Western blot analysis showed an approximately four-
278 fold increase of MIC15 expression in strain MIC15-iKD compared to the TATi parental line (Fig 4C).
279 As determined by quantitative real-time PCR, this upregulation was paralleled by 2.8-fold higher
280 levels of MIC15 mRNA (Fig 4D). In MIC15-iKD parasites grown in presence of 0.5 μg/ml Atc for
281 various time periods, Western blot analysis revealed a marked reduction of MIC15 expression
282 after 24 h, with the protein dropping to undetectable levels from the 29 h time point onwards (Fig
283 4C). Accordingly, IFA demonstrated that Atc treatment of the knockdown strain caused the loss of
284 MIC15 expression (Fig 4E). Of notice, untreated MIC15-iKD parasites exhibited an evident
285 perinuclear staining compared to the parental strain, indicative of protein accumulation in the
286 endoplasmic reticulum (Fig 4E and S4 Fig). This is likely due to increased *MIC15* expression under
287 the control of the constitutive TRE/S4 promoter. To evaluate the overall impact of MIC15

288 depletion on the tachyzoite lytic cycle we carried out plaque assays in which HFF monolayers were
289 infected with 250 tachyzoites of either the TATi parental strain or the MIC15-iKD mutant. Unlike
290 the parental strain, MIC15-iKD tachyzoites displayed a normal plaque forming ability only in
291 absence of Atc treatment but were unable to form plaques in presence of the drug, even using a
292 10-fold higher parasite inoculum (Fig 4F). This marked defect was fully restored by
293 complementation of the mutant with an extra-copy of the wild type *MIC15* gene (Figs 4G and 4H;
294 S5 Fig).
295

296 Secretory organelle localization and microneme discharge are not 297 affected by MIC15 deficiency

298 The strong phenotype displayed by the knockdown strain upon Atc treatment suggested that
299 MIC15 is involved in one or more key steps underlying the tachyzoite lytic cycle. This prompted us
300 to dissect this complex process by a series of observational and functional assays. The replication
301 rate of MIC15-iKD parasites was compared to that of the parental strain by counting the number
302 of tachyzoites per vacuole at 24 h after pulse infection of HFF monolayers (S6A Fig). This assay
303 showed similar distribution of vacuole size irrespective of parasite pretreatment with Atc for 60
304 hrs, indicating that MIC15 loss has no influence on tachyzoite division. Also the efficiency of conoid
305 extrusion, a calcium-dependent process which occurs during gliding, invasion and egress, was
306 evaluated with a specific test. Extracellular parasites were incubated in a medium containing or
307 not the calcium ionophore A23187, fixed and microscopically scored for the presence or absence
308 of conoid protrusion. No significant difference was observed between MIC15-depleted and control
309 tachyzoites of the TATi and MIC15-iKD strains (S6B Fig).

310 Using confocal IFA we explored the possibility that MIC15 downregulation might grossly
311 alter the biogenesis or positioning of the tachyzoite secretory organelles, which orchestrate the

312 interaction with the host cell at multiple levels. To this end, MIC15-iKD tachyzoites treated or not
313 with Atc for 60 hrs were dual stained with serum MIC15Nt together with mAbs recognizing either
314 MIC2 or MIC8, known to be targeted to distinct subpopulations of micronemes [30], the rhoptry
315 marker ROP5 or the dense granule protein GRA1. As shown in Figs 5A-D, all selected proteins
316 appeared comparably abundant and correctly localized in both strains and regardless of Atc
317 treatment. Furthermore, the efficiency of microneme discharge was investigated by Western blot
318 by detecting MIC2, MIC4 and MIC8 in the ESA fraction of parasites unstimulated or treated with
319 1% ethanol to induce microneme discharge. As shown in Fig 5E, this non quantitative assay
320 showed that the supernatant of TATi and MIC15-iKD strains contained comparable levels of the
321 three microneme markers irrespective of MIC15 expression. A normal microneme functionality
322 was indirectly suggested also by two distinct in vitro assays that measured the ability of
323 tachyzoites to glide on a solid substrate or egress from the host cell upon stimulation with 2 μM of
324 the calcium ionophore A23187. Both processes, which are strictly dependent on the secretion of
325 specific micronemal effectors such as MIC2 [21] and PLP1 [31], respectively, were shown to occur
326 with equal efficiency in the parental strain and in MIC15-iKD parasites regardless of Atc treatment
327 (Figs 5F and 5G). Collectively, these results demonstrate that MIC15 downregulation does not
328 affect microneme secretion.
329

330 MIC15 depletion dramatically inhibits host cell invasion

331 The inability of MIC15-depleted tachyzoites to produce plaques in human fibroblasts was further
332 investigated in vitro by measuring the efficiency of active host cell penetration by TATi and MIC15-
333 iKD parasites. To this end, the two strains were grown for 60 hrs in presence or absence of Atc and
334 used to infect HFF monolayers for 20 min at 37°C. After removal of free exracellular tachyzoites by
335 extensive washing, the cultures were fixed with 4% paraformaldehyde and invaded (intracellular)

336 versus attached (extracellular) parasites were enumerated by differential IFA using a red-green
337 assay [18]. As shown in Fig 6A, Atc treatment of MIC15-iKD tachyzoites significantly reduced
338 invasion by approximately 80% compared to the untreated control and the parental strain.
339 Noteworthy, this marked inhibition was not accompanied by a reduction in the number of
340 attached MIC15-iKD parasites, which rather showed a significant increase upon MIC15 depletion.
341 This result excluded that the strong MIC15-iKD phenotype was due to the impairment of host cell
342 attachment, strongly indicating a relation to molecular events occurring downstream along the
343 invasion process.
344

345 MIC14 expression restores the invasion defect in MIC15-depleted 346 tachyzoites

347 In order to explore the existence of possible compensatory mechanisms capable to
348 counterbalance the loss of fitness due to MIC15 downregulation, the evolution of the non invasive
349 phenotype was studied over time in MIC15-iKD tachyzoites grown in presence of Atc for up to 120
350 days. Surprisingly, we found that as soon as 36 days after the start of the Atc treatment, parasites
351 depleted in MIC15 were able to produce sporadic and very small areas of lysis (Fig 7A), compared
352 to the null plaque count of MIC15-iKD tachyzoites treated with Atc for the standard 2.5 days
353 before the plaque assay. Restoration of the lytic phenotype became more evident after 120 days
354 of continuous growth with Atc, as shown by the increased number of lytic events and the
355 formation of distinctly larger plaques, though reduced in size compared to parasites grown in
356 absence of Atc during the assay (Fig 7A). To investigate the possible involvement of the MIC15
357 paralog, MIC14, in the restored lytic ability, tachyzoites treated with Atc for 120 days were
358 subjected to limiting dilution cloning in presence of the drug. Seven independent clones were
359 isolated and screened by Western blot with the mouse serum T148 raised against a recombinant

360 fragment of the MIC14 ectodomain (Fig 2A). As shown in Fig 7B for a representative clone
361 denominated MIC15-iKD/MIC14^R, the polyclonal antibody specifically detected a high molecular
362 weight product which was absent in the parental strains TATi and MIC15-iKD and exhibited a
363 molecular mass compatible with the 253 kDa predicted for MIC14. To validate the hypothesis that
364 the newly identified protein corresponded to MIC14, we successfully knocked out the
365 corresponding gene in MIC15-iKD/MIC14^R tachyzoites by replacing the first two exons and
366 upstream region of *MIC14* with a TUB/CAT resistance cassette (Fig 7C). Western blot analysis with
367 serum T148 showed that MIC15-iKD/MIC14^R/MIC14KO parasites lacked the high MW band
368 characteristic of the parental strain, which was unequivocally identified as MIC14. This result was
369 corroborated by the return of MIC15-iKD/MIC14^R/MIC14KO parasites to the null plaque
370 phenotype of the parental line (Fig 7E). The analysis of MIC15-iKD/MIC14^R strain by RT-qPCR using
371 a primer pair mapping to exon 16 of the complete gene showed that the upregulation of MIC14
372 and the consequent rescue of the lytic phenotype was associated with a 12.7-fold increase of the
373 full-length *MIC14* mRNA (Fig 7F). The sequencing of 2.3 kb upstream of the MIC14 translation start
374 codon of both MIC15-iKD and MIC15-iKD/MIC14^R strains excluded the presence of mutations that
375 could be linked to the observed transcriptional upregulation.

376 Attempts to immunolocalize MIC14 in MIC15-iKD/MIC14^R tachyzoites using serum T148
377 were unsuccessful. This prompted us to engineer this strain by endogenously tagging the *MIC14*
378 gene by insertion of three C-terminal Ty epitopes, obtaining the MIC14^R-3xTy line (Fig 8A). To
379 enhance the expression level of the tagged protein, we also generated the strain TUB-MIC14^R-3xTy
380 by replacing the *MIC14* endogenous promoter with the constitutive promoter of *T. gondii* α-
381 tubulin (Fig 8A). Western blot analysis by anti-Ty antibodies showed expression in both mutant
382 strains of the □250 kDa full-length MIC14 and confirmed that TUB-MIC14^R-3xTy parasites
383 produced higher amounts of the tagged protein (Fig 8B). Moreover, anti-Ty antibodies revealed

384 the presence in both mutants of two additional bands of approximately 180 and 100 kDa,
385 suggesting that MIC14 undergoes proteolytic processing at two distinct sites in the extracellular
386 domain of the molecule. Consistent with the Western blot result, MIC14 was localized much more
387 efficiently by the anti-Ty mAb in TUB-MIC14^{R}-3xTy parasites, in which the tagged protein displayed
388 the same diffuse cytoplasmic distribution of MIC15 (Fig 8C). Taken together, these data
389 demonstrate that MIC15 depletion can favour the emergence of parasite variants overexpressing
390 MIC14 and that this protein, undetectable in wild type tachyzoites, has a MIC15-like punctate
391 localization and can partially compensate the pronounced invasion defect due to MIC15 loss.
392

393 MIC15 and MIC14 are involved in rhoptry secretion

394 To gain insight in the mechanism involved in the impairment of invasion consequent to MIC15
395 depletion, we explored the possible impact of this condition on rhoptry discharge, which is crucial
396 to moving junction formation and host cell penetration. Rhoptry secretion was investigated by an
397 evacuole assay, consisting in an invasion assay performed in presence of Cytochalasin D (CytD).
398 Under this condition, actin polymerization and therefore parasite invasion are inhibited, without
399 interfering with the ability of extracellular tachyzoites to inject in the host cell cytoplasm small
400 lipid vesicles enriched in rhoptry bulb proteins (evacuoles). The detection of evacuoles by IFA using
401 an anti-ROP1 antibody was used as an indicator of correct rhoptry secretion by parasites attached
402 to the host cell surface. Notably, depletion in MIC15 dramatically reduced evacuole formation by
403 Atc treated MIC15-iKD parasites if compared to the untreated control and the TATi parental strain
404 (Fig 9), and to levels comparable to tachyzoites depleted in RON5, key protein in the moving
405 junction complex formation [32]. On the contrary, Atc treated strain MIC15-iKD/MIC14^{R} did not
406 present the evacuole defect, further supporting the compensatory effect of MIC14 upregulation.
407 Importantly, transmission electron microscopy observations of MIC15-iKD tachyzoites showed that

408 MIC15 downregulation did not cause ultrastructural anomalies in the apical positioning of the
409 rhoptries (S7 Fig). Collectively, our results demonstrate that the paralogous proteins MIC15 and
410 MIC14 are novel components of a *T. gondii* molecular pathway controlling rhoptry exocytosis.
411 Consistent with their newly revealed function, we propose to adopt a more appropriate
412 nomenclature and to rename MIC15 as rhoptry discharge factor 1 (RDF1) and MIC14 as rhoptry
413 discharge factor 2 (RDF2).
414

415 # Discussion

416 Apicomplexan parasites exhibit a lineage-specific expansion of genes encoding thrombospondin-
417 related proteins [33-35], whose functional role has been more widely investigated in *Plasmodium*
418 spp. In the present work we explored the repertoire of *Toxoplasma gondii* adhesive proteins
419 containing the TSP1 domain and showed that two novel members of this family, RDF1 (MIC15) and
420 RDF2 (MIC14), are implicated in rhoptry discharge. While this process has remained poorly
421 understood for decades, recent studies shed novel light on this crucial secretory event. According
422 to the current ultrastructural model [3], a couple of *T. gondii* rhoptries at a time are primed for
423 secretion by docking their necks through the conoid and in proximity of an Apicomplexa-specific
424 apical vesicle (AV) anchored to the cytosolic face of the PM. Four similar vesicles are aligned to the
425 intraconoidal microtubules and are presumed to serve for successive rounds of secretion. The
426 anchoring of the AV to the parasite PM was recently shown to be mediated by the rhoptry
427 secretory apparatus, a highly elaborated structure described also in the distantly related
428 apicomplexan *Cryptosporidium parvum,* that includes an apical rosette embedded in the parasite
429 PM and electrondense proteinaceous material bridging the rosette to the AV. The rosette, which
430 consists of eight peripheral particles and a central one resembling a pore, is the rhoptry secretion

431 site and is evolutionarily conserved in the Alveolata superphylum, being implicated in the
432 exocytosis of the extrusomes of free-living ciliates [36].

433 Rhoptry discharge factors 1 and 2 add to the narrow group of *T. gondii* proteins so far
434 linked to rhoptry exocytosis. Unlike microneme secretion, which can be induced by artificially
435 raising parasite intracellular [Ca^{2+}], rhoptry discharge strictly requires the contact with the host
436 cell. Although the nature of the initial external trigger remains obscure, the micronemal proteins
437 MIC8 [26] and AMA1 [37] are know to be involved, as their downregulation significantly impairs
438 rhoptry discharge. Within the parasite, RASP2, a member of the rhoptry apical surface proteins
439 (RASPs), was shown to be essential for rhoptry secretion in both *T. gondii* and *Plasmodium*
440 *falciparum* [38]. By locally enhancing phosphatidic acid and phosphoinositides concentration,
441 RASP2 is presumed to be involved in the docking of the rhoptries and fusion of their membrane
442 with that of the AV. A major advance in the definition of the molecular machinery governing
443 rhoptry exocytosis was the recent identification of a new class of *T. gondii* proteins evolutionarily
444 conserved throughout the Alveolata. Aquilini et al. [2021] identified *T. gondii* orthologs of Non-
445 discharge (Nd) proteins known to be essential for trichocyst exocytosis and rosette formation in
446 *Paramecium tetraurelia* [39,40]. In *T. gondi,* Nd6 and Nd9 were shown to form a complex that
447 includes five additional proteins, i.e, two other Nd molecules conserved in Ciliata named TgNdp1
448 and TgNdp2, the calcium-sensing protein TgFER2 [25] belonging to the ferlin family and essential
449 for rhoptry secretion, a putative GTPase and a Coccidia-specific hypothetical protein. Conditional
450 depletion of each of the four TgNd proteins significantly reduced rhoptry secretion leading to
451 severe invasion deficiency, that in Nd1, Nd2 and Nd9 iKD lines was paralleled by defective rosette
452 assembly. In addition to sharing with Nd1, Nd9 and TgFER2 a similar dotted distribution
453 throughout the tachyzoite cytoplasm, Nd2 and Nd6 were also shown to accumulate at the AV. In
454 accordance with the functional characteristics of individual Nd complex partners, it has been

455 suggested that calcium signalling and nucleotide binding/hydrolysis are instrumental to rosette
456 assembly and/or rhoptry exocytosis [2].

457 In contrast to all TSP1 domain-containing proteins so far characterized in the Apicomplexa,
458 RDF1 and RDF2 display an unprecedented intracellular localization and no evidence of trafficking
459 to the micronemes. The lack of relation to these organelles is further supported by spatial
460 hyperLOPIT data [41] showing that RDF1 is part of a separate minicluster including another
461 member of the thrombospondin family (TGME49_277910) and two TM multipass proteins as yet
462 uncharacterized (TGGT1_261080, TGGT1_292020), whose localization and possible interaction
463 with RDF1 and RDF2 will deserve additional study. The punctate cytoplasmic distribution of RDF1
464 and RDF2 is strikingly similar to that reported for TgFER2 [25] and individual TgNd proteins [2] and
465 is suggestive of a dynamic situation. However, such a dispersed localization is not evocative of
466 known vesicular trafficking routes or intracellular structures. Our attempts to clarify this point by
467 immunoelectron microscopy localization of RDF1 produced inconsistent results, as previously
468 reported for TgFER2 [25].

469 The present study revealed that the two RDF paralogs act along the rhoptry discharge
470 signalling pathway, whose structure and underlying mechanisms are only starting to be elucidated.
471 Future studies should evaluate the colocalization of RDF1 and RDF2 with members of the Nd
472 protein complex and the possible impact of RDF1/RDF2 depletion on the ultrastructure of the
473 rhoptry secretory apparatus and apical vesicles, as well as on Nd proteins localization. Unlike Nd2
474 and Nd6, IFA did not support the accumulation of RDF1 or RDF2 at the parasite apex, however, the
475 presence of the proteins in amounts below the detection limit of light microscopy cannot be
476 excluded. One possibility is that RDF1 and RDF2 are part of the machinery that tightly controls
477 membrane fusion between the rhoptries and the AV and/or between the AV and the parasite PM.
478 The adhesive domains of the RDF paralogs might be involved in the formation of multiprotein

479 complexes with unknown partners by mediating binding to carbohydrate moieties or direct
480 protein-protein interactions. Therefore, important functional clues may derive from
481 immunoprecipitation experiments with anti-RDF1/anti-RDF2 antibodies aimed at the identification
482 of possible interactors. The presence at the N-terminus of RDF1 and RDF2 of a typical leader
483 peptide or a signal-anchor sequence, respectively, is predictive of protein targeting to the
484 endoplasmic reticulum. Further research is needed to understand under which form and by which
485 mechanism the two proteins are translocated to the parasite cytosol and if their trafficking is
486 mediated by a not yet defined membranous system.

487 The characterization of RDF1 and RDF2 uncovered an example of *T. gondii* phenotypic
488 plasticity related to rhoptry exocytosis. The functional redundancy of genes crucial for parasite
489 survival is a strategy widely used by microorganism including the Apicomplexa, which have to face
490 diverse environmental changes during their life cycles [42]. In *P. falciparum*, extensive phenotypic
491 plasticity was documented by the identification of hyerarchically organized invasion pathways
492 relying on the EBA and PfRh redundant families of merozoite surface antigens [43]. In *T. gondii*,
493 several adaptive mechanisms have been described which are able to counteract mutations
494 detrimental for parasite fitness, with most examples being related to host cell invasion. These
495 include MyoA [28], a major component of the subpellicular glidosome, that is responsible for the
496 retrograde translocation of surface microneme adhesins and crucially involved in invasion and
497 egress [44]. MyoA knockout and knockdown mutants were shown to possess a 16-25% residual
498 invasion capability that was attributed to the compensatory action of MyoC, normally associated
499 with a distinct glidosome localized to the basal polar ring. In MyoA-KO parasites, MyoC was shown
500 to rapidly redistribute along the parasite inner membrane complex and to functionally rescue the
501 loss of MyoA. A second compensatory mechanism was demonstrated in tachyzoites lacking
502 GAP80, that is functionally replaced by the MyoA anchoring protein GAP45, in recruiting MyoC to

503 the posterior glidosome [45]. A series of compensatory mechanisms enhance the capability of *T.*
504 *gondii* to form a functional moving junction. This essential invasion-related structure depends on
505 the interaction between the rhoptry neck protein RON2 and the micronemal AMA1 exposed on
506 the host cell and parasite PM, respectively [6,7]. It was shown that AMA1 ablation by gene
507 excision is compensated by the transcriptional upregulation of the RON2-binding paralog AMA2
508 [46,47]. Furthermore, the generation of a double knockout mutant AMA1-KO/AMA2-KO revealed
509 that the divergent AMA1 homolog AMA4, which is abundantly expressed in the sporozoite stage,
510 is upregulated in the tachyzoite along with its specific ligand $RON2_{L1}$ [48], thus providing a second
511 line compensatory mechanism preserving a molecular interaction of pivotal importance for
512 parasite survival. To our knowledge, none of the molecular mechanisms underlying the mentioned
513 compensatory systems has been elucidated.

514 Our results confirmed the expression of a *RDF2* mRNA form of □4.5 Kb consistent with
515 the TGME49_218310 ToxoDB gene model. Furthermore, we showed that RH tachyzoites express a
516 second and much longer *RDF2* transcript that could be detected only by amplification techniques.
517 Importantly, this allowed to unveil the so far unpredicted structure of the full-length *RDF2* gene
518 and to demostrate that it harbors two promoter regions. In wild type tachyzoites, the □4.5 Kb
519 mRNA transcribed from the downstream promoter is the dominating form. The predicted encoded
520 protein of 968 amino acids was neither detected by anti-RDF2 polyclonal antibodies in Western
521 blot, nor identified by mass-spectrometry in published *T. gondii* proteomic studies. This lack of
522 proteomic data is likely to reflect very low expression levels of full-length RDF2 and the possible
523 instability of the short RDF2 form, that in absence of an N-terminal leader sequence might be
524 released in the cytoplasm and degraded.

525 The expression of a RDF2 form of □250 kDa predicted in the present study was
526 demonstrated by Western blot detection, whose specificity was indicated by the disappearance of

527 this band upon knocking out of the encoding gene in MIC15-iKD/MIC14^R parasites. The emergence
528 of a variant strain in which full-length RDF2 upregulation partially compensated RDF1 depletion
529 raised the question as to which mechanism is implicated in this rapid adaptation. We speculate
530 that the mechanism regulating the activity the two *RDF2* promoters and accounting for the 12.7-
531 fold increase of the long *RDF2* mRNA in MIC15-iKD/MIC14^R parasites might involve epigenetic
532 control by specific antisense RNAs. Although their role in apicomplexan parasites remains largely
533 unexplored, non coding RNA species are associated with more than 20% of *T. gondii* [49] and
534 *Plasmodium* [50] open reading frames. Our hypothesis is based on the observation that some *T.*
535 *gondii* strains represented in ToxoDB show peaks of antisense transcription in the region
536 encompassing the *RDF2* downstream promoter. While scarcely represented in strain RH, these
537 *RDF2* antisense RNA(s) are more abundant in *T. gondii* strains showing a concomitant increase of
538 sense RNA peaks indicating a higher degree of expression of the full lenght *RDF2* gene. A possible
539 explanation is that the rate of transcription initiation at the *RDF2* downstream promoter is
540 repressed by the binding of complementary antisense RNA(s), thus favouring the activity of the
541 upstream promoter. Further experimental work will be required to explore the levels of the *RDF2*
542 antisense transcripts in MIC15-iKD/MIC14^R parasites compared to the parental strain, and to
543 characterize the RNA species possibly involved in the modulation of *RDF2* expression.

544 In conclusion, our findings show the unprecedented involvement of two thrombospondin-
545 related proteins in rhoptry exocytosis and expand current knowledge of the molecular players
546 acting along the pathway that regulates this critical invasion-related process. In addition, the
547 demonstration of structural/functional homology between RDF1 and RDF2 uncovers a further
548 adaptation mechanism enhancing *T. gondii* phenotypic plasticity.

549

550 # Materials and methods

551 ## Ethics statement

552 Animals were housed and maintained at the Animal Care Unit of the Istituto Superiore di Sanità
553 (ISS) in Italy according to D.L.gs. n. 26/2014 (art. 26 of D.L.gs.n.26/14). The in vivo protocol (n.
554 972/2017-PR; 11/12/2017) was approved by the Italian Ministry of Health.

555

556 ## Parasites

557 *Toxoplasma gondii* tachyzoites of strains RH*Δku80* and TATiΔ*ku80* [29] were grown in human
558 foreskin fibroblasts (HFF) monolayers in Dulbecco's modified Eagle's medium (DMEM) with
559 GlutaMAX (Gibco) supplemented with 10% Nu-Serum (Gibco), 10 mM HEPES (N-2-hydroxy-
560 ethylpiperazine-N'-2-ethanesulfonic acid) and penicillin/stretptomycin at 37°C in a humid 5% CO_2
561 atmosphere. Tachyzoites from actively lysing HFF cultures were recovered by passage through a
562 27-gauge syringe needle and purified by a 3-μm membrane filter.

563

564 ## Generation of parasite strains

565 Parasite transfections were carried out as previously described [51]. Primers used in this study
566 are listed in S1 Table.

567 To generate the vector *pMIC15-iKD-TRE/S4*, genomic fragments of 1269 and 1176 bp
568 located upstream and downstream of the MIC15 promoter of *T. gondii* RH strain were amplified
569 with primers P44/P45 and P46/P47, respectively. The TRE/S4 cassette for the replacement of the
570 *MIC15* promoter was amplified from plasmid *pDt7S4* [52] using the primer pair P48/P49. The
571 upstream sequence, the TRE/S4 cassette and the downstream sequence were cloned sequentially
572 in the *Eco*RV-*Apa*I, *Bam*H1-*Spe*I and *Spe*I-*Sac*II restriction sites of a modified version of *pTUB5-*

573 *DHFR* [51], in which an additional *Eco*RV restriction site was added upstream of the resistance
574 marker.

575 The complementing vector *pMIC15-comp-CAT* was generated by amplifying the *MIC15*
576 cDNA coding region from strain RHΔ*ku80* using the primers P13 and P14. The 8960 bp amplicon
577 was cut with the restriction enzymes *Xba*I and *Pac*I and cloned in the corresponding restriction
578 sites upstream of the 3'UTR of the *GRA2* gene, already present in the acceptor plasmid. A region
579 of 2065 bp encompassing the *MIC15* promoter was then amplified from RHΔ*ku80* genomic DNA
580 with primers P15/P16 and cloned between the *Not*I and *Xba*I restriction sites upstream of the
581 *MIC15* coding region. Finally, the *TUB-CAT* resistance cassette was amplified from the *pTUB5-CAT*
582 plasmid using the primers P17 and P18 and inserted in the *Asc*I and *Not*I restriction sites
583 upstream of the *MIC15* minigene, obtaining plasmid *pMIC15-comp-CAT*. The vector was
584 sequenced to rule out the occurrence of nucleotide substitutions. The complementing vector was
585 then linearized at the *Xcm*I restriction site and transfected in the MIC15-iKD strain for integration
586 by single crossing over upstream of the tetracycline-controlled *MIC15* locus. The correct
587 integration of the complementing plasmid was assessed by PCR using the primer pairs P25/P26
588 and P27/P28 (S5 Fig).

589 To produce the knockout construct pMIC14KO, a genomic region of approximately 1.1 kb
590 lying upstream of the *MIC14* promoter and one spanning exons 4 and 5 of *MIC14*, were amplified
591 from RHΔ*ku80* genomic DNA with the primer pairs P9/10 and P11/P12, respectively. The two
592 amplicons were cloned in the *pTub5/CAT* plasmid [53] 5' and 3' to the *CAT* gene, using the
593 restriction sites *Apa*I/*Hin*dIII and *Spe*I/*Not*I, respectively. The *Not*I linearized plasmid was
594 introduced into the MIC15-iKD/MIC14^{R} strain to replace the promoter and the 5'-terminal exons
595 with the *CAT* cassette by double homologous recombination. Transfected parasites were selected

596 with 20 µM chloramphenicol and cloned, obtaining strain MIC15-iKD/MIC14^{R}KO/MIC14KO. The
597 occurrence of the correct recombination event was tested by PCR (Fig 7D).

598 To generate strain MIC15-smMYC the *MIC15* gene was endogenously tagged by inserting
599 the sequence encoding the spaghetti monster-c-myc (smMYC) protein in the second exon of
600 *MIC15*. The sequence encoding the smMYC tag was amplified from plasmid *pLIC-SMGFP_MYC*
601 [54] with primers P55 and P56, containing at the 5' end 40 bp sequences lying upstream and
602 downstream of the selected *MIC15* insertion point, respectively. Insertion of the smMYC epitope
603 between amino acids 29 and 30 was obtained by co-transfecting RHΔ*ku80* tachyzoites with the
604 amplified smMYC repair template and a CRISPR/Cas9 vector encoding the Cas9 endonuclease,
605 and containing the bleomycin resistance gene and the *MIC15*-specific gRNA sequence 5'-
606 GUAACUUGUCAACUGCAGUU-3'. Twenty-four hours post transfection parasites were
607 mechanically extruded from HFF and treated for 4 h with 50 µg/ml of bleomycin at 37˚C to enrich
608 for parasites harboring the CRISPR/Cas9 vector. Bleomycin-treated parasites were allowed to
609 expand in HFF monolayer and then cloned by limiting dilution into 96-well plates. Identification of
610 clones carrying the correct integration of the smMYC tag was carried out as described [55] using
611 primer pairs P57/59 or P58/P47.

612 Insertion of the Ty epitope upstream of the MIC15 TM region (between amino acids 2688
613 and 2689) was obtained by co-transfecting RHΔ*ku80* tachyzoites with a Ty repair template along
614 with a CRISPR/Cas9 vector encoding the Cas9 endonuclease, and containing the *MIC15*-specific
615 gRNA sequence 5'-AUCGAUCUUUCCGAAGCUUC-3' and the bleomycin resistance cassette. The
616 repair template was generated by annealing the complementary 110 bp long oligonucleotides
617 P29 and P30 [56], and consisted of the Ty coding sequence flanked by 40 bp long genomic regions
618 lying upstream and downstream of the selected *MIC15* insertion point. Following the bleomycin

619 selection procedure described above for the MIC15-smMYC strain, individual parasite clones
620 were screened for the correct integration of the TY tag using primer pairs P1/P2 or P3/P4.

621 Strain MIC15-2xHA was generated by endogenously tagging the 3' end of *MIC15* in
622 RH*Δku80* tachyzoites by single homologous recombination, using plasmid *pMIC15-2xHA-DHFR*. A
623 DNA sequence of □1.3 kb spanning exons 41 and 42 of *MIC15* was amplified from the RH*Δku80*
624 genome with primers P60 and P61, containing the restriction sites *Eco*RV and *Pac*I, respectively.
625 In addition, primer P61 encoded two tandemly repeated HA epitopes followed by a stop codon. A
626 second genomic fragment encompassing the 3'UTR of the *DHFR* gene was amplified with primers
627 P62 and P63, which carried the restriction sites *Pac*I and *Apa*I, respectively. Exploiting the
628 common *Pac*I restriction site, the two amplicons were tandemly cloned in the *Eco*RV and *Apa*I
629 restriction sites of a modified version of *pTUB5-DHFR* [51]. Following transfection with *Bst*EII-
630 linearized plasmid *pMIC15-2xHA-DHFR* and pyrimethamine selection, parasite clones were
631 screened for the C-terminal insertion of 2xHA epitopes using primers P75 and P63.

632 Strain MIC15-iKD/MIC14^{R}-3xTy was generated by endogenously tagging the 3' end of
633 *MIC14* with three consecutive Ty epitopes in MIC15-iKD/MIC14^{R} parasites. A genomic sequence
634 of □1.0 kb spanning exons 42 and 43 of *MIC14* was amplified with primers P70 and P71
635 harboring the restriction sites *Not*I and *Sph*I, respectively. A second PCR product, encompassing
636 the sequence coding for 3xTy epitopes and the 3'UTR of SAG1, was obtained from plasmid *DGK2-*
637 *3xTy* (gently donated by Dominique Soldati-Favre, University of Geneva) using primers P68 and
638 P69, which carried the restriction sites *Sph*I and *Bam*HI, respectively. Exploiting the common *Sph*I
639 restriction site, the two amplicons were tandemly cloned in the *Not*I and *Bam*H1 sites of *pTUB5-*
640 *CAT.* The resulting plasmid *pMIC14-3xTy* was linearized at the *Nhe*I restriction site and introduced
641 in strain MIC15-iKD/MIC14^{R} by single homologous recombination. Individual parasite clones were
642 screened for the correct recombination event by PCR using primers P72 and P69.

643 Strain TUB-MIC14^{R}-3xTy was obtained in MIC15-iKD/MIC14^{R}-3xTy parasites by a single
644 homologous recombination event that replaced the *MIC14* endogenous promoter with that of
645 the *β-tubulin* gene. Using primers P73 and P74, a DNA sequence of 1200 bp spanning *MIC14*
646 from the translation initiation codon to the second exon was amplified from the RH*Δku80*
647 genome and cloned downstream of the TUB promoter of plasmid pGRA1-NAT1_TUB [57],
648 exploiting the restriction sites *Eco*RI and *Xba*I. Following transfection with the resulting plasmid
649 *pTUB/MIC14-3xTY-NAT* linearized at the *Hpa*I restriction site and two rounds of selection of
650 extracellular tachyzoites with 500 μg/ml of nourseothricin, parasites were cloned by limiting
651 dilution and screened with the diagnostic primers P43 and P73.
652

653 **Analysis of full-length cDNAs**

654 The full length cDNAs of *MIC14* and *MIC15* were reconstructed by combining the sequences of
655 polyadenylated cDNA clones isolated from a tachyzoite library, with those of overlapping RT-PCR
656 and 5' RACE products. A λZAPII cDNA library of strain RH (NIH AIDS Research and Reference
657 Reagent Program) was screened by limiting dilution [27] using the oligonucleotide pairs P5/P6 for
658 *MIC14* and P7/P8 for *MIC15*. The 5' end regions of *MIC14* and *MIC15* were amplified using the
659 SMART RACE cDNA Amplification Kit (Clontech BD) using total or poly(A)$^{+}$ tachyzoite RNA (strain
660 RH) as starting material. For amplification of the *MIC14* 5' end, 1.5 μg of poly(A)$^{+}$ tachyzoite RNA
661 was reverse transcribed with random examers prior to PCR amplification with the *MIC14* primer
662 P43 and the nested universal primer included in the kit. For amplification of the 5' end of *MIC15*,
663 1.5 μg of total RNA was reverse transcribed with primer P39 prior to PCR amplication of the RT
664 product with the *MIC15* nested primer P40 and the nested universal primer provided with the kit.
665 The *MIC14* cDNA region encompassing the full length gene from exon 2 to exon 29 was amplified

666 from reverse transcribed poly(A)$^+$ RNA using the primer pair P41/P42. Individual 5' RACE and RT-
667 PCR products were cloned into the pCR2.1 TA cloning vector (Invitrogen) and sequenced.
668

669 Antibodies

670 Antibodies directed against *T. gondii* proteins or epitope tags used in this study and the relative
671 dilutions used in Western blot and immunofluorescence analyses are described in S2 Table.
672 Rabbit polyclonal antibodies MIC15Nt and MIC15Ct were raised against recombinant fragments
673 of MIC15 spanning amino acids 928-1460 and 2494-2706, respectively. Mouse polyclonal serum
674 T148 was raised against the MIC14 region encompassing amino acids 1761-1996. Recombinant
675 protein fragments were produced in *Escherichia coli* (strain M15) as fusion products with an N-
676 terminal tag of six histidines using plasmid pQE30 (Qiagen) and purified from total bacterial
677 lysates by nickel affinity chromatography. The anti-MIC15 monoclonal antibody 22E6 was
678 produced as previously described [58] using as immunogen the same protein fragment employed
679 to obtain rabbit serum MIC15Nt.
680

681 Quantitative real-time PCR

682 Total tachyzoite RNA was extracted using the RNeasy Plus Mini kit (Qiagen) and treated with Turbo
683 DNA free kit (Ambion) to remove residual genomic DNA. Following RNA quantification with the
684 Qubit RNA HS assay kit (Invitrogen) and inspection of RNA integrity by agarose gel electrophoresis,
685 0.5-1 µg of total RNA was reverse transcribed using Protoscript II Reverse Transcriptase (New
686 England Biolabs). Quantitative real-time PCR was carried out using the Light-Cycler 480 SYBR
687 Green I Master (Roche). Each 20 µl reaction contained 10 µl of 2x SYBER Green I Master mix, 20
688 pmol of each primer and 4 µl of cDNA (diluted 1:20). One pre-incubation step (5 min, 95°C) was
689 followed by 45 cycles of denaturation (10 sec, 95°C), annealing (10 sec, 58°C) and elongation (10

690 sec, 72°C) performed on a LyghtCycler 96 Instrument (Roche). *MIC14* and *MIC15* transcripts were
691 amplified with the primer pairs P64/P65 and P66/P67. Relative levels of *MIC14* and *MIC15* mRNAs
692 with respect to the β-tubulin mRNA internal control were calculated using the $2^{-\Delta\Delta Ct}$ method. All
693 samples were analyzed in triplicate using both biological and technical replicates.
694

695 Western blot analysis

696 Excreted-secreted antigens (ESA) were prepared as described below in the paragraph on
697 microneme secretion. Total protein lysates were obtained by incubating purified *T. gondii*
698 tachyzoites in RIPA buffer (150 mM NaCl, 1% NP-40, 0.5% sodium deoxycholate, 0.1% SDS, 50
699 mM Tris–HCl pH 8.0) for 20 min on ice and removing insoluble material by centrifugation at 3000
700 x g for 20 min at 4°C.. Parasite proteins were reduced with 200 μM dithiotreitol (DTT) and
701 separated on 4-12% NuPAGE Bis-Tris gels (Thermo Fisher Scientific). Following wet protein
702 transfer to nitrocellulose, the filters were blocked for 1 hr with 5% skimmed milk (Sigma-Aldrich)
703 in 2x Tris Buffered Saline/Tween 20 (20 mM Tris–HCl pH 8.0, 300 mM NaCl, 0.1% Tween 20) and
704 subsequently incubated for 1 hr with primary antibodies at dilutions reported in S2 Table.
705 Reactive bands were visualised using goat anti-mouse IgG or goat anti-rabbit IgG secondary
706 antibodies conjugated to horseradish peroxidase (Invitrogen) and the LiteAblot Plus Enhanced
707 Chemiluminescent Substrate (EuroClone).
708

709 Immunofluorescence analysis

710 Indirect immunofluorescence assays were performed on extracellular *T. gondii* tachyzoites or
711 parasite-infected HFF monolayers grown for 24-30 h at 37°C on 12 mm glass coverslips or in 8-well
712 chamber slides. The samples were fixed for 10 min with 4% formaldehyde, quenched with 0.1 M

713 glycine/PBS, permeabilized with 0.5% Triton X-100 if required and blocked for 1 h with 2% fetal
714 bovine serum in PBS. Incubation with primary antibodies diluted in 2% fetal bovine serum in PBS
715 was carried out for 1 hr at dilutions reported in S2 Table. Bound primary antibodies were detected
716 using 1:500-1:2000 dilutions of goat anti-mouse or goat anti-rabbit IgG secondary antibodies
717 conjugated with Alexa Fluor 488 or Alexa Fluor 594 (Invitrogen). Tachyzoite and HFF nuclei were
718 labelled with DAPI (4',6'-diamidino-2-phenylindole). Samples were mounted in SlowFade Antifade
719 reagent (Invitrogen) and stored at 4°C in the dark. Confocal images were taken by a Zeiss LSM 980
720 confocal microscope (Zeiss, Germany), using a planapo objective 60x oil A.N. 1,42. Images
721 recorded have an optical thickness of 0.4 μm. Other images were taken by an Axioplan 2
722 epifluorescence microscope (Zeiss, Germany) using a 100 x oil immersion objective and an
723 Axiocam digital camera using the Zeiss Axiovision 4.7 software.
724

725 Microneme secretion assay

726 To obtain the excreted-secreted antigen (ESA) fraction, freshly egressed tachyzoites grown ± Atc
727 for 60 hrs were resuspended in DMEM/10 mM HEPES at a concentration of $2x10^9$ parasites/ml
728 and incubated for 20 min at 37°C with or without 1% ethanol to stimulate microneme secretion
729 [59]. Following parasite centrifugation at 1000 g for 10 min at 4°C, the pellet fraction was
730 collected and extracted with RIPA buffer, the supernatant was centrifuged at 2000 g for 5 min at
731 4°C to remove residual tachyzoites. The supernatant, representing the ESA fraction, was
732 concentrated using Centricon 20 Plus concentrators (Millipore) and stored at -80°C for further
733 use. Pellet and ESA protein amounts equivalent to $1.2x10^7$ or $4x10^7$ parasites, respectively, were
734 analyzed by SDS gel electrophoresis on NuPAGE™ 4-12% Bis-Tris gels (Thermo Fisher Scientific)
735 and blotted.
736

737 ## Plaque assay

738 Freshly egressed tachyzoites cultivated ± Atc for 60 hrs were used to infect HFF monolayers in 6-
739 well plates. Infected cultures were grown ± Atc for nine days before fixation with cold methanol
740 and staining with crystal violet.

741

742 ## Conoid extrusion assay

743 Conoid extrusion ability was assessed in parasites grown ± Atc for 60 hrs and incubated for 30
744 sec with 3 μM of calcium ionophore A23187 in DMSO or absolute DMSO as control. Following
745 fixation with 4% paraformaldehyde (PFA), parasites were deployed on glass slides and scored for
746 conoid protrusion by phase contrast microscopy. Percentage of tachyzoites with extruded
747 conoids was determined by counting 200 parasites per condition in three independent
748 experiments conducted in triplicate.

749

750 ## Replication assay

751 Freshly egressed parasites grown ± Atc for 60 hrs were used to infect HFF monolayers for 20 min
752 in chamber slides. After removal of uninvaded tachyzoites, the cultures were incubated ± Atc for
753 24 h prior to fixation with 4% PFA. Intracellular parasites were stained with anti-GAP45 antibodies
754 and DAPI and the number of parasites per vacuole was determined, counting 100 vacuoles for
755 each condition in 3 independent experiments performed in triplicate.

756

757 ## Invasion-attachment assay

758 Freshly egressed parasites grown ± Atc for 60 hrs were resuspended in DMEM, 2% NuSerum, 10
759 mM HEPES and seeded on confluent HFF monolayers in 8-well chamber slides (Eppendorf) at a

760 density of $5x10^5$ tachyzoites/well. Following centrifugation at 100 g for 2 min at 4°C, the cultures
761 were incubated at 37°C for 20 min to allow host cell attachment and invasion, washed with
762 DMEM to remove free extracellular parasites and fixed with 4% PFA. Samples were analyzed by
763 differential IFA using a red-green assay [18]. Briefly, to label exclusively attached (extracellular)
764 tachyzoites, non permeabilized samples were incubated with an anti-SAG1 mAb followed by
765 Alexa 488-conjugated anti-mouse IgG antibodies (Invitrogen). After permeabilization with 0.5%
766 Triton X-100 (Sigma-Aldrich), all parasites were stained with rabbit anti-GRA1 antibodies followed
767 by 594-conjugated anti-rabbit IgG antibodies. Attached (green+red) and invaded (red) tachyzoites
768 were enumerated by examining 30 microscopic fields/well at 630x magnification. The data shown
769 are representative of four independent experiments performed in triplicate.
770

771 ## Evacuole assay

772 Rhoptry proteins discharge was tested using the evacuole detection assay, as previously
773 described [8]. Briefly, parasites grown for 48 h ± Atc were collected by syringe lysis of HFF
774 monolayers, washed in ice-cold DMEM, resuspended in DMEM supplemented with 1µM
775 Cytochalasin D (Sigma-Aldrich) and incubated on ice for 10 min. Pre-chilled HFF monolayers in
776 DMEM/1µM Cytochalasin D were infected with $8x10^6$ parasites per glass coverslips, centrifuged
777 at 1100 g for 1 min and allowed to settle on ice for 20 min. The medium was replaced with pre-
778 warmed growth medium containing 1µM Cytochalasin D and cultures were incubated for 20 min
779 at 37°C in a water bath. Following fixation with 4% PFA, dual IFA was performed using rabbit anti-
780 GAP45 antibodies to visualize the tachyzoites and an anti-ROP1 mAb to detect evacuoles. Results
781 are representative of three independent experiments performed in triplicate.
782

783 ## Induced egress assay

784 Freshly harvested parasites grown ± Atc for 60 hrs were used to infect HFF cultures on 12 mm
785 glass coverslips. After 30 h of growth ± Atc, infected cultures were washed with PBS, incubated
786 for 2 min at 37°C in 2 μM calcium ionophore A23187 diluted in Hank's Balanced Salt Solution and
787 fixed with 4% PFA. Egressed versus non egressed vacuoles were scored by IFA staining the
788 parasites with an anti-SAG1 mAb and parasitophorous vacuole membranes with rabbit anti-GRA7
789 antibodies. The percentage of egressed vacuoles was determined in three independent
790 experiments conducted in triplicate by counting 100 vacuoles for each experimental condition.
791

792 ## Gliding motility assay

793 Intracellular parasites grown ± Atc for 60 hrs were mechanically extruded from HFF monolayers,
794 resuspended in Hank's Balanced Salt Solution and seeded in 8-well poly-Lysine-coated (0.025%;
795 Sigma-Aldrich) chamber slides (Falcon) at a density of 200,000 parasites/well. Following
796 centrifugation at 100 g for 2 min, parasites were incubate for 30 min at 37°C ± Atc, fixed with 4%
797 PFA and surface stained with an anti-SAG1 mAb to reveal fluorescent SAG1 trails. Results are
798 representative of three independent experiments carried out in triplicate.
799

800 ## Transmission Electron Microscopy

801 Freshly egressed tachyzoites grown ± Atc for 60 hrs were fixed with 4% paraformaldehyde/0.1%
802 glutaraldehyde in 0.1 M sodium cacodylate buffer overnight at 4°C. Next, the suspensions were
803 gently washed in buffer, dehydrated in ethanol serial dilutions and embedded in LR White,
804 medium-grade acrylic resin (London Resin Company, UK). The samples were polymerised in a
805 55°C oven for 48 h and ultrathin sections, obtained by an UC6 Ultramicrotome (Leica), were
806 collected on gold grids, stained by uranyl acetate 2% in H_2O for 10 min and examined at 100kV by

807 EM 208S Transmission Electron Microscope (FEI - Thermo Fisher) equipped with the acquisition
808 system Megaview SIS camera (Olympus).
809

810 Bionformatic tools

811 Genome-wide homology searches were performed using the PSI-BLAST and BLASTP algorithms
812 (https://blast.ncbi.nlm.nih.gov), multiple amino acid sequence comparisons with CLUSTAL Omega
813 (https://www.ebi.ac.uk/Tools/msa/clustalo/). Leader peptide and TM regions were predicted
814 with the programs SignalP 5.0 (https://services.healthtech.dtu.dk/service.php?SignalP-5.0) and
815 TMHMM 2.0 (https://services.healthtech.dtu.dk/service.php?TMHMM-2.0), respectively. Protein
816 domain architecture was analyzed with the Simple Modular Architecture Research Tool (SMART;
817 http://smart.embl-heidelberg.de/) and by interrogating the Pfam (https://pfam.xfam.org/) and
818 NCBI CDD (https://www.ncbi.nlm.nih.gov/Structure/cdd/cdd.shtml) databases. Phylogenetic
819 analyses were performed with the MEGA 11 software, using MIC14 and MIC15 amino acid
820 sequences aligned with the MUSCLE software.
821

822 Statistical analysis

823 Statistical analyses were carried out with Prism 9 (GraphPad Software Inc., La Jolla, CA, USA)
824 using Student's t tests as indicated in the figure legends. All assays were performed in triplicate
825 and results are shown as mean values ±SEM of at least three independent biological replicates.
826 Differences were considered significant if P values were <0.05.
827

828 Supporting information

829 **S1 Fig. Sequence homology between MIC14 and MIC15.** The full length amino acid sequences of

830 the two proteins were aligned with Clustal Omega. Conserved amino acids are boxed in yellow,
831 invariable cysteine residues are highlighted in red. The main amino acids domains or elements are
832 indicated by horizontal bars according the following color code: TSP1 domain (red), H-lectin
833 domain (grey), transmembrane region (blue), leader peptide (green), signal-anchor sequence
834 (orange).
835
836 **S2 Fig. Comparison of the MIC14 and MIC15 transmembrane domains of *Toxoplasma gondii* and**
837 **other Coccidia with those of characterized transmembrane microneme proteins.** MIC14 and
838 MIC15 amino acid sequences from other Coccidia are from *Neospora caninum*, *Hammondia*
839 *hammondi*, *Besnoitia besnoiti*, *Cyclospora cayetanensis, Cystoisospora suis* and *Eimeria acervulina.*
840 The amino acid alignment includes the C-terminal transmembranes of the micronemal proteins
841 MIC2, MIC6, MIC8, MIC12, MIC16, AMA1, AMA2, AMA3 and AMA4 of *T. gondii* and TRAP of
842 *Plasmodium falciparum*. The amino acid sequences of the transmembrane domains are shown in
843 grey, characterized and predicted rhomboid cleavage sites in yellow. Invariable amino acid
844 residues located in the MIC14 and MIC15 cytoplasmic tails immediately downstream of the
845 transmembrane domain are highlighted in green.
846
847 **S3 Fig. Endogenous tagging and localization of MIC15. (A)** Schematic representation of three
848 MIC15 variants in which the tags smMYC, Ty or HA were introduced at the N-terminus, upstream
849 of the TMD or at the C-terminus, respectively. **(B)** Western blots showing recognition of the
850 differently tagged MIC15 proteins by the relative anti-tag mAb and by the anti-MIC15 rabbit serum
851 MIC15Nt. The dense granule protein GRA1 or the inner membrane complex protein GAP45 were
852 used as loading controls. **(C)** Immunofluorescence localization of Ty- and HA-tagged MIC15
853 variants in intracellular tachyzoites stained with the corresponding anti-epitope mAb. For the

854 localization of smMYC-tagged MIC15 see Fig 3D. Nuclei are stained with DAPI. Scale bars, 5 μm.

855

856 **S4 Fig. Dual immunofluorescence analysis of MIC15-iKD tachyzoites.** Staining of intracellular

857 MIC15-iKD parasites with anti-MIC15 mAb 22E6 and rabbit serum MIC15Nt showing colocalization

858 of the two fluorescent signals.

859

860 **S5 Fig. Creation and validation of genetically complemented MIC15iKD parasites**. **(A)** Schematics

861 of single crossover integration to restore expression of *MIC15* via genetic complementation with

862 plasmid *pMIC15-comp-CAT* containing the *MIC15* minigene (in grey). Single crossover integration

863 was directed to the *MIC15-iKD* locus via homologous regions indicated in orange. Primers used to

864 assess integration of the complementation construct are shown as numbered arrows. **(B)** PCR

865 analysis of integration at the *MIC15-iKD* locus using primers shown in (A) and reported in S1 Table.

866 Migration of size standards in kilobase pairs (Kbp) is shown to the right.

867

868 **S6 Fig. Phenotypic analysis of MIC15-iKD strain. (A)** Intracellular growth of MIC15-iKD and

869 TATi tachyzoites cultivated for 60 hrs in presence or absence of Atc prior to pulse infection of HFF

870 cells. At 24 h post infection the cultures were fixed with PFA and the number of parasites per

871 vacuole was determined. The graph shows for each strain and condition the percentage of

872 vacuoles containing 2, 4, 8 or 16 tachyzoites. Values represent means ± SEM of three experiments

873 carried out in triplicate. Statistical analysis by the Student's two tailed *t*-test did not reveal

874 significant differences. **(B)** Conoid extrusion assay on MIC15-iKD and TATi tachyzoites cultivated ±

875 Atc for 60 hrs. The graph reports the percentage of tachyzoites with conoid protrusion following

876 incubation with 3 μM of calcium ionophore A23187 or DMSO as control. Values represent means ±

877 SEM of three experiments carried out in triplicate. Statistical analysis was performed by the

878 Student's two tailed *t*-test and showed no significant differences.

879

880 **S7 Fig. Ultrastructural analysis of rhoptries in MIC15-iKD tachyzoites.** Electron micrographs of the
881 apical region of MIC15-iKD parasites grown in absence (A) or presence (B) of Atc for 60 hrs. The
882 arrows indicate the correct intraconoidal positioning of the rhoptry neck (Rn) irrespective of
883 MIC15 depletion. Rhoptry bulbs (Rb) are also shown. The conoid is indicated by a white
884 arrowhead. Scale bar, 500 nm. The presence of colloidal gold particles should not be considered.

885

886 **S8 Fig. Alignment of MIC14 and MIC15 amino acid sequences used to generate the phylogenetic**
887 **tree.** The amino acid sequences of MIC14 and MIC15 orthologs are identified by the following
888 accession numbers: *Toxoplasma gondii*, MIC14 (AY089992), MIC15 (DQ459408); *Besnoita besnoiti*,
889 MIC14 (XP_029221473), MIC15 (XP_029222264); *Cyclospora cayetanensis*, MIC14
890 (XP_026191791), MIC15 (XP_026191793); *Cystoisospora suis*, MIC14 (PHJ15367), MIC15,
891 (PHJ22147); *Eimeria acervulina*, MIC14 (XP_013251268), MIC15 (XP_013251270); *Hammondia*
892 *hammondi*, MIC14, (HHA_218310), MIC15, (HHA_247195); *Neospora caninum*, MIC14 (CEL70510),
893 MIC15 (CEL70693); *Sarcocystis neurona*, MIC15 (SN3_00200915).

894

895 # Acknowledgments

896 We wish to thank Drs Vern B. Carruthers (University of Michigan, US), Dominique Soldati-Favre
897 (University of Geneva, Switzerland) and Maryse Lebrun (University of Montpellier, France) for
898 kindly providing critical reagents and for helpful discussion.

899 # Author Contributions

900 **Conceptualization**: Furio Spano, Manlio Di Cristina

Data curation: Furio Spano

Formal analysis: Furio Spano, Matteo Lunghi

Investigation: Furio Spano, Alessia Possenti, Manlio Di Cristina, Chiara Nicastro, Matteo Lunghi, Valeria Messina, Federica Piro, Lorenzo Tramontana, Simona Cherchi, Mario Falchi, Lucia Bertuccini

Methodology: Furio Spano, Manlio Di Cristina

Project administration: Furio Spano

Supervision: Furio Spano, Manlio Di Cristina

Writing - original draft: Furio Spano, Manlio Di Cristina

Writing - review & editing: Furio Spano, Manlio Di Cristina, Alessia Possenti, Matteo Lunghi

Data Availability Statement

The full-length sequence of MIC14 is available in GenBank with accession number AY089992. The full-length sequence of MIC15 is available in GenBank with accession number DQ459408.

Financial Disclosure Statement.

This work was partially supported by the European Commission's Directorate-General for Health and Food Safety (DG SANTE) - European Reference Laboratory for the Parasites, grant agreement no. SI2.801980.The study was also conducted with support from the University of Perugia Fondo Ricerca Di Base 2019 program of the Department of Chemistry, Biology and Biotechnology (MDC, ML and FP).

Competing interests.

The authors have declared that no competing interests exist.

References

1. Dos Santos Pacheco N, Tosetti N, Koreny L, Waller RF, Soldati-Favre D. Evolution, composition, assembly, and function of the conoid in Apicomplexa. Trends Parasitol. 2020 Aug;36(8):688-704. doi: 10.1016/j.pt.2020.05.001. Epub 2020 May 31. PMID: 32487504.

2. Aquilini E, Cova MM, Mageswaran SK, Dos Santos Pacheco N, Sparvoli D, Penarete-Vargas DM, et al. An alveolata secretory machinery adapted to parasite host cell invasion. Nat Microbiol. 2021; 6(4):425-434. doi: 10.1038/s41564-020-00854-z PMID: 33495622

3. Mageswaran SK, Guérin A, Theveny LM, Chen WD, Martinez M, Lebrun M, Striepen B, Chang YW. In situ ultrastructures of two evolutionarily distant apicomplexan rhoptry secretion systems. Nat Commun. 2021; 12(1):4983. doi: 10.1038/s41467-021-25309-9 PMID: 34404783

4. Dubois DJ, Soldati-Favre D. Biogenesis and secretion of micronemes in *Toxoplasma gondii*. Cell Microbiol. 2019; 21(5):e13018. doi: 10.1111/cmi.13018. Erratum in: Cell Microbiol. 2019 Oct;21(10):e13105 PMID: 30791192

5. Ben Chaabene R, Lentini G, Soldati-Favre D. Biogenesis and discharge of the rhoptries: key organelles for entry and hijack of host cells by the Apicomplexa. Mol Microbiol. 2021; 115(3):453-465. doi: 10.1111/mmi.14674 PMID: 33368727

6. Alexander DL, Mital J, Ward GE, Bradley P, Boothroyd JC. Identification of the moving junction complex of *Toxoplasma gondii*: a collaboration between distinct secretory organelles. PLoS Pathog. 2005; 1(2):e17. doi: 10.1371/journal.ppat.0010017 PMID: 16244709

7. Besteiro S, Michelin A, Poncet J, Dubremetz JF, Lebrun M. Export of a *Toxoplasma gondii* rhoptry neck protein complex at the host cell membrane to form the moving junction during invasion. PLoS Pathog. 2009; 5(2):e1000309. doi: 10.1371/journal.ppat.1000309 PMID: 19247437

8. Håkansson S, Charron AJ, Sibley LD. *Toxoplasma* evacuoles: a two-step process of secretion and fusion forms the parasitophorous vacuole. EMBO J. 2001; 20(12):3132-44. doi: 10.1093/emboj/20.12.3132 PMID: 11406590

9. Adams JC, Tucker RP. The thrombospondin type 1 repeat (TSR) superfamily: diverse proteins with related roles in neuronal development. Dev Dyn. 2000; 218(2):280-99. doi: 10.1002/(SICI)1097-0177(200006)218:2<280::AID-DVDY4>3.0.CO;2-0 PMID: 10842357.

10. Nardin EH, Nussenzweig V, Nussenzweig RS, Collins WE, Harinasuta KT, Tapchaisri P, et al. Circumsporozoite proteins of human malaria parasites *Plasmodium falciparum* and *Plasmodium vivax*. J Exp Med. 1982; 156(1):20-30. doi: 10.1084/jem.156.1.20 PMID: 7045272

11. Robson KJ, Hall JR, Jennings MW, Harris TJ, Marsh K, Newbold CI, et al. A highly conserved amino-acid sequence in thrombospondin, properdin and in proteins from sporozoites and blood stages of a human malaria parasite. Nature. 1988; 335(6185):79-82. doi: 10.1038/335079a0 PMID: 3045563

971 12. Trottein F, Triglia T, Cowman AF. Molecular cloning of a gene from *Plasmodium falciparum* that
972 codes for a protein sharing motifs found in adhesive molecules from mammals and plasmodia.
973 Mol Biochem Parasitol. 1995; 74(2):129-41. doi: 10.1016/0166-6851(95)02489-1 PMID:
974 8719155
975
976 13. Baum J, Richard D, Healer J, Rug M, Krnajski Z, Gilberger TW, et al. A conserved molecular motor
977 drives cell invasion and gliding motility across malaria life cycle stages and other apicomplexan
978 parasites. J Biol Chem. 2006; 281(8):5197-208. doi: 10.1074/jbc.M509807200 PMID: 16321976
979
980 14. Thompson J, Cooke RE, Moore S, Anderson LF, Janse CJ, Waters AP. PTRAMP; a conserved
981 *Plasmodium* thrombospondin-related apical merozoite protein. Mol Biochem Parasitol. 2004;
982 134(2):225-32. doi: 10.1016/j.molbiopara.2003.12.003 PMID: 15003842
983
984 15. Moreira CK, Templeton TJ, Lavazec C, Hayward RE, Hobbs CV, Kroeze H, et al. The *Plasmodium*
985 TRAP/MIC2 family member, TRAP-Like Protein (TLP), is involved in tissue traversal by
986 sporozoites. Cell Microbiol. 2008; 10(7):1505-16. doi: 10.1111/j.1462-5822.2008.01143.x PMID:
987 18346224
988
989 16. Combe A, Moreira C, Ackerman S, Thiberge S, Templeton TJ, Ménard R. TREP, a novel protein
990 necessary for gliding motility of the malaria sporozoite. Int J Parasitol. 2009; 39(4):489-96. doi:
991 10.1016/j.ijpara.2008.10.004 PMID: 19000911
992
993 17. Klug D, Frischknecht F. Motility precedes egress of malaria parasites from oocysts. Elife. 2017;
994 6:e19157. doi: 10.7554/eLife.19157 PMID: 28115054
995
996 18. Huynh MH, Rabenau KE, Harper JM, Beatty WL, Sibley LD, Carruthers VB. Rapid invasion of host
997 cells by *Toxoplasma* requires secretion of the MIC2-M2AP adhesive protein complex. EMBO J.
998 2003; 22(9):2082-90. doi: 10.1093/emboj/cdg217 PMID: 12727875
999
1000 19. Opitz C, Di Cristina M, Reiss M, Ruppert T, Crisanti A, Soldati D. Intramembrane cleavage of
1001 microneme proteins at the surface of the apicomplexan parasite *Toxoplasma gondii*. EMBO J.
1002 2002; 21(7):1577-85. doi: 10.1093/emboj/21.7.1577 PMID: 11927542
1003
1004 20. Sheiner L, Santos JM, Klages N, Parussini F, Jemmely N, Friedrich N, et al. *Toxoplasma gondii*
1005 transmembrane microneme proteins and their modular design. Mol Microbiol. 2010; 77(4):912-
1006 29. doi: 10.1111/j.1365-2958.2010.07255.x PMID: 20545864
1007
1008 21. Huynh MH, Carruthers VB. *Toxoplasma* MIC2 is a major determinant of invasion and virulence.
1009 PLoS Pathog. 2006; 2(8):e84. doi: 10.1371/journal.ppat.0020084 PMID: 16933991
1010
1011 22. Gras S, Jackson A, Woods S, Pall G, Whitelaw J, Leung JM, et al. Parasites lacking the micronemal
1012 protein MIC2 are deficient in surface attachment and host cell egress, but remain virulent *in*
1013 *vivo*. Wellcome Open Res. 2017; 2:32. doi: 10.12688/wellcomeopenres.11594.2 PMID:
1014 28630943
1015
1016 23. Huynh MH, Liu B, Henry M, Liew L, Matthews SJ, Carruthers VB. Structural basis of *Toxoplasma*
1017 *gondii* MIC2-associated protein interaction with MIC2. J Biol Chem. 2015; 290(3):1432-41. doi:
1018 10.1074/jbc.M114.613646 PMID: 25411252

1019
1020 24. Sidik SM, Huet D, Ganesan SM, Huynh MH, Wang T, Nasamu AS, et al. A genome-wide CRISPR
1021 screen in *Toxoplasma* identifies essential apicomplexan genes. Cell. 2016; 166(6):1423-
1022 1435.e12. doi: 10.1016/j.cell.2016.08.019 PMID: 27594426
1023
1024 25. Coleman BI, Saha S, Sato S, Engelberg K, Ferguson DJP, Coppens I, et al. A member of the ferlin
1025 calcium sensor family is essential for *Toxoplasma gondii* rhoptry secretion. mBio. 2018;
1026 9(5):e01510-18. doi: 10.1128/mBio.01510-18 PMID: 30279285
1027
1028 26. Kessler H, Herm-Götz A, Hegge S, Rauch M, Soldati-Favre D, Frischknecht F, et al. Microneme
1029 protein 8--a new essential invasion factor in *Toxoplasma gondii*. J Cell Sci. 2008;121: 947-956.
1030 doi: 10.1242/jcs.022350 PMID: 18319299
1031
1032 27. Israel DI. A PCR-based method for high stringency screening of DNA libraries. Nucleic Acids Res.
1033 1993; 21(11):2627-2631. doi: 10.1093/nar/21.11.2627 PMID: 8332459
1034
1035 28. Meissner M, Schlüter D, Soldati D. Role of *Toxoplasma gondii* myosin A in powering parasite
1036 gliding and host cell invasion. Science. 2002; 298(5594):837-40. doi: 10.1126/science.1074553
1037 PMID: 12399593
1038
1039 29. Sheiner L, Demerly JL, Poulsen N, Beatty WL, Lucas O, Behnke MS, et al. A systematic screen to
1040 discover and analyze apicoplast proteins identifies a conserved and essential protein import
1041 factor. PLoS Pathog. 2011; 7(12):e1002392. doi: 10.1371/journal.ppat.1002392 PMID:
1042 22144892
1043
1044 30. Kremer K, Kamin D, Rittweger E, Wilkes J, Flammer H, Mahler S, et al. An overexpression screen
1045 of *Toxoplasma gondii* Rab-GTPases reveals distinct transport routes to the micronemes. PLoS
1046 Pathog. 2013; 9(3):e1003213. doi: 10.1371/journal.ppat.1003213 PMID:23505371
1047
1048 31. Kafsack BF, Pena JD, Coppens I, Ravindran S, Boothroyd JC, Carruthers VB. Rapid membrane
1049 disruption by a perforin-like protein facilitates parasite exit from host cells. Science. 2009;
1050 323(5913):530-3. doi: 10.1126/science.1165740 PMID: 19095897
1051
1052 32. Beck JR, Chen AL, Kim EW, Bradley PJ. RON5 is critical for organization and function of the
1053 *Toxoplasma* moving junction complex. PLoS Pathog. 2014; 10(3):e1004025. doi:
1054 10.1371/journal.ppat.1004025 PMID: 24651769
1055
1056 33. Naitza S, Spano F, Robson KJ, Crisanti A. The thrombospondin-related protein family of
1057 Apicomplexan parasites: the gears of the cell invasion machinery. Parasitol Today. 1998;
1058 14(12):479-84. doi: 10.1016/s0169-4758(98)01346-5 PMID: 17040860
1059
1060 34. Deng M, Templeton TJ, London NR, Bauer C, Schroeder AA, Abrahamsen MS. *Cryptosporidium*
1061 *parvum* genes containing thrombospondin type 1 domains. Infect Immun. 2002; 70(12):6987-
1062 95. doi: 10.1128/IAI.70.12.6987-6995.2002 PMID: 12438378
1063
1064 35. Montenegro VN, Paoletta MS, Jaramillo Ortiz JM, Suarez CE, Wilkowsky SE. Identification and
1065 characterization of a *Babesia bigemina* thrombospondin-related superfamily member, TRAP-1:
1066 a novel antigen containing neutralizing epitopes involved in merozoite invasion. Parasit Vectors.

1067 2020; 13(1):602. doi: 10.1186/s13071-020-04469-5 PMID: 33261638
1068
1069 36. Gubbels MJ, Duraisingh MT. Evolution of apicomplexan secretory organelles. Int J Parasitol.
1070 2012; 42(12):1071-81. doi: 10.1016/j.ijpara.2012.09.009 PMID: 23068912
1071
1072 37. Mital J, Meissner M, Soldati D, Ward GE. Conditional expression of *Toxoplasma gondii* apical
1073 membrane antigen-1 (TgAMA1) demonstrates that TgAMA1 plays a critical role in host cell
1074 invasion. Mol Biol Cell. 2005; 16(9):4341-9. doi: 10.1091/mbc.e05-04-0281 PMID: 16000372
1075
1076 38. Suarez C, Lentini G, Ramaswamy R, Maynadier M, Aquilini E, Berry-Sterkers L, et al. A lipid-
1077 binding protein mediates rhoptry discharge and invasion in *Plasmodium falciparum* and
1078 *Toxoplasma gondii* parasites. Nat Commun. 2019; 10(1):4041. doi: 10.1038/s41467-019-11979-
1079 z PMID: 31492901
1080
1081 39. Froissard M, Keller AM, Dedieu JC, Cohen J. Novel secretory vesicle proteins essential for
1082 membrane fusion display extracellular-matrix domains. Traffic. 2004; 5(7):493-502. doi:
1083 10.1111/j.1600-0854.2004.00194.x PMID: 15180826
1084
1085 40. Gogendeau D, Keller AM, Yanagi A, Cohen J, Koll F. Nd6p, a novel protein with RCC1-like
1086 domains involved in exocytosis in *Paramecium tetraurelia*. Eukaryot Cell. 2005; 4(12):2129-39.
1087 doi: 10.1128/EC.4.12.2129-2139.2005 PMID: 16339730
1088
1089 41. Barylyuk K, Koreny L, Ke H, Butterworth S, Crook OM, Lassadi I, et al. A comprehensive
1090 subcellular atlas of the *Toxoplasma* proteome via hyperLOPIT provides spatial context for
1091 protein functions. Cell Host Microbe. 2020; 28(5):752-766.e9. doi: 10.1016/j.chom.2020.09.011
1092 PMID: 33053376
1093
1094 42. Frénal K, Soldati-Favre D. Plasticity and redundancy in proteins important for *Toxoplasma*
1095 invasion. PLoS Pathog. 2015; 11(8):e1005069. doi: 10.1371/journal.ppat.1005069 PMID:
1096 26270966
1097
1098 43. Baum J, Maier AG, Good RT, Simpson KM, Cowman AF. Invasion by *P. falciparum* merozoites
1099 suggests a hierarchy of molecular interactions. PLoS Pathog. 2005; 1(4):e37. doi:
1100 10.1371/journal.ppat.0010037 PMID: 16362075
1101
1102 44. Frénal K, Dubremetz JF, Lebrun M, Soldati-Favre D. Gliding motility powers invasion and egress
1103 in Apicomplexa. Nat Rev Microbiol. 2017; 15(11):645-660. doi: 10.1038/nrmicro.2017.86 PMID:
1104 28867819
1105
1106 45. Frénal K, Marq JB, Jacot D, Polonais V, Soldati-Favre D. Plasticity between MyoC- and MyoA-
1107 glideosomes: an example of functional compensation in *Toxoplasma gondii* invasion. PLoS
1108 Pathog. 2014; 10(10):e1004504. doi: 10.1371/journal.ppat.1004504 PMID: 25393004
1109
1110 46. Bargieri DY, Andenmatten N, Lagal V, Thiberge S, Whitelaw JA, Tardieux I, et al. Apical
1111 membrane antigen 1 mediates apicomplexan parasite attachment but is dispensable for host
1112 cell invasion. Nat Commun. 2013; 4:2552. doi: 10.1038/ncomms3552 PMID: 24108241
1113
1114 47. Poukchanski A, Fritz HM, Tonkin ML, Treeck M, Boulanger MJ, Boothroyd JC. *Toxoplasma gondii*

1115 sporozoites invade host cells using two novel paralogues of RON2 and AMA1. PLoS One. 2013;
1116 8(8):e70637. doi: 10.1371/journal.pone.0070637 PMID: 23940612
1117
1118 48. Lamarque MH, Roques M, Kong-Hap M, Tonkin ML, Rugarabamu G, Marq JB, et al. Plasticity and
1119 redundancy among AMA-RON pairs ensure host cell entry of *Toxoplasma* parasites. Nat
1120 Commun. 2014; 5:4098. doi: 10.1038/ncomms5098 PMID: 24934579
1121
1122 49. Radke JR, Behnke MS, Mackey AJ, Radke JB, Roos DS, White MW. The transcriptome of
1123 *Toxoplasma gondii*. BMC Biol. 2005; 3:26. doi: 10.1186/1741-7007-3-26 PMID: 16324218
1124
1125 50. Siegel TN, Hon CC, Zhang Q, Lopez-Rubio JJ, Scheidig-Benatar C, Martins RM, et al. Strand-
1126 specific RNA-seq reveals widespread and developmentally regulated transcription of natural
1127 antisense transcripts in *Plasmodium falciparum*. BMC Genomics. 2014; 15(1):150. doi:
1128 10.1186/1471-2164-15-150 PMID: 24559473
1129
1130 51. Afonso C, Paixão VB, Klaus A, Lunghi M, Piro F, Emiliani C, et al. *Toxoplasma*-induced changes in
1131 host risk behaviour are independent of parasite-derived AaaH2 tyrosine hydroxylase. Sci Rep.
1132 2017; 7(1):13822. doi: 10.1038/s41598-017-13229-y. PMID: 29062106
1133
1134 52. van Dooren GG, Tomova C, Agrawal S, Humbel BM, Striepen B. *Toxoplasma gondii* Tic20 is
1135 essential for apicoplast protein import. Proc Natl Acad Sci U S A. 2008; 105(36):13574-9. doi:
1136 10.1073/pnas.0803862105 PMID: 18757752
1137
1138 53. Soldati D, Boothroyd JC. Transient transfection and expression in the obligate intracellular
1139 parasite *Toxoplasma gondii*. Science. 1993; 260(5106):349-52. doi: 10.1126/science.8469986
1140 PMID: 8469986
1141
1142 54. Hortua Triana MA, Márquez-Nogueras KM, Chang L, Stasic AJ, Li C, Spiegel KA, et al. Tagging of
1143 weakly expressed *Toxoplasma gondii* calcium-related genes with high-affinity tags. J Eukaryot
1144 Microbiol. 2018; 65(5):709-721. doi: 10.1111/jeu.12626 PMID: 29672999
1145
1146 55. Piro F, Carruthers VB, Di Cristina M. PCR screening of *Toxoplasma gondii* single clones directly
1147 from 96-well plates without DNA purification. Methods Mol Biol. 2020; 2071:117-123. doi:
1148 10.1007/978-1-4939-9857-9_6 PMID: 31758449
1149
1150 56. Di Cristina M, Carruthers VB. New and emerging uses of CRISPR/Cas9 to genetically manipulate
1151 apicomplexan parasites. Parasitology. 2018; 145(9):1119-1126. doi:
1152 10.1017/S003118201800001X PMID: 29463318
1153
1154 57. Van Tam T, Rooney PJ, Knoll LJ. Nourseothricin acetyltransferease: a positive selectable marker
1155 for *Toxoplasma gondii*. J Parasitol. 2006; 92(3):668-70. doi: 10.1645/GE-706R.1 PMID:
1156 16884024
1157
1158 58. Possenti A, Cherchi S, Bertuccini L, Pozio E, Dubey JP, Spano F. Molecular characterisation of a
1159 novel family of cysteine-rich proteins of *Toxoplasma gondii* and ultrastructural evidence of
1160 oocyst wall localisation. Int J Parasitol. 2010; 40(14):1639-49. doi: 10.1016/j.ijpara.2010.06.009
1161 PMID: 20708619
1162

1163 59. Carruthers VB, Giddings OK, Sibley LD. Secretion of micronemal proteins is associated with
1164 *Toxoplasma* invasion of host cells. Cell Microbiol. 1999; 1(3):225-35. doi: 10.1046/j.1462-
1165 5822.1999.00023.x PMID: 11207555
1166
1167 60. Achbarou A, Mercereau-Puijalon O, Autheman JM, Fortier B, Camus D, Dubremetz JF.
1168 Characterization of microneme proteins of *Toxoplasma gondii*. Mol Biochem Parasitol. 1991;
1169 47(2):223-33. doi: 10.1016/0166-6851(91)90182-6 PMID: 1944419.
1170
1171 61. Reiss M, Viebig N, Brecht S, Fourmaux MN, Soete M, Di Cristina M, Dubremetz JF, Soldati D.
1172 Identification and characterization of an escorter for two secretory adhesins in *Toxoplasma*
1173 *gondii*. J Cell Biol. 2001; 152(3):563-78. doi: 10.1083/jcb.152.3.563 PMID: 11157983
1174
1175 62. Meissner M, Reiss M, Viebig N, Carruthers VB, Toursel C, Tomavo S, et al. A family of
1176 transmembrane microneme proteins of *Toxoplasma gondii* contain EGF-like domains and
1177 function as escorters. J Cell Sci. 2002; 115(Pt 3):563-74. doi: 10.1242/jcs.115.3.563 PMID:
1178 11861763
1179
1180 63. Tartarelli I, Tinari A, Possenti A, Cherchi S, Falchi M, Dubey JP, et al. During host cell traversal
1181 and cell-to-cell passage, *Toxoplasma gondii* sporozoites inhabit the parasitophorous vacuole
1182 and posteriorly release dense granule protein-associated membranous trails. Int J Parasitol.
1183 2020; 50(13):1099-1115. doi: 10.1016/j.ijpara.2020.06.012 PMID: 32882286
1184
1185 64. Sibley LD, Niesman IR, Parmley SF, Cesbron-Delauw MF. Regulated secretion of multi-lamellar
1186 vesicles leads to formation of a tubulo-vesicular network in host-cell vacuoles occupied by
1187 *Toxoplasma gondii*. J Cell Sci. 1995; 108 (Pt 4):1669-77. doi: 10.1242/jcs.108.4.1669 PMID:
1188 7615684
1189
1190 65. Dunn JD, Ravindran S, Kim SK, Boothroyd JC. The *Toxoplasma gondii* dense granule protein GRA7
1191 is phosphorylated upon invasion and forms an unexpected association with the rhoptry
1192 proteins ROP2 and ROP4. Infect Immun. 2008; 76(12):5853-61. doi: 10.1128/IAI.01667-07
1193 PMID: 18809661
1194
1195 66. Dogga SK, Mukherjee B, Jacot D, Kockmann T, Molino L, Hammoudi PM, et al. A druggable
1196 secretory protein maturase of *Toxoplasma* essential for invasion and egress. Elife. 2017;
1197 6:e27480. doi: 10.7554/eLife.27480 PMID: 28898199
1198
1199 67. Couvreur G, Sadak A, Fortier B, Dubremetz JF. Surface antigens of *Toxoplasma gondii*.
1200 Parasitology. 1988; 97 (Pt 1):1-10. doi: 10.1017/s0031182000066695 PMID: 3174230
1201
1202

1203 # Figure captions

1204

1205 **Fig 1. Structure of the *MIC14* and *MIC15* genomic loci and analysis of *MIC14* transcription.**

1206 Schematic representation of the ToxoDB gene models of *MIC15* **(A)** and *MIC14* with the adjacent

1207 *TGME49_218340* **(B)**. Predicted exons are shown as red (*MIC15*) or blue (*MIC14* and

1208 *TGME49_218340*) boxes, untranslated regions as yellow boxes, intronic sequences as black lines.
1209 The numbers at the extremes of the gene models correspond to the nucleotidic positions on
1210 chromosome XII. Cloned cDNAs, RT-PCR amplicons or 5'RACE products are represented as red,
1211 green or blue dashed lines, respectively. The position of the primers used for transcript
1212 amplification is indicated by black arrows. **(C)** Structure of the complete *MIC14* locus as deduced
1213 from the combined sequence resulting from the overlap between a library derived cDNA, RT-PCR
1214 and 5' RACE products. The grey bars indicate the exons spanned by the two probes used for
1215 Northern blot hybridizations. **(D)** Northern blot analysis of tachyzoite total RNA with the *MIC14*
1216 probes P5' and P3'. Exposure time, 96 hours.
1217
1218 **Fig 2. Phylogenetic analysis and domain organization of MIC14 and MIC15. (A)** Unrooted
1219 maximum likelihood phylogenetic tree of MIC14 and MIC15 proteins in Apicomplexa. Bootstrap
1220 values for 1000 trials are shown. The amino acid alignment used to generate the tree is shown in
1221 S8 Fig. Amino acid sequences used to generate the phylogenetic tree are identified by the
1222 following accession numbers: *Toxoplasma gondii*, MIC14 (AY089992), MIC15 (DQ459408);
1223 *Besnoita besnoiti*, MIC14 (XP_029221473), MIC15 (XP_029222264); *Cyclospora cayetanensis*,
1224 MIC14 (XP_026191791), MIC15 (XP_026191793); *Cystoisospora suis*, MIC14 (PHJ15367), MIC15,
1225 (PHJ22147); *Eimeria acervulina*, MIC14 (XP_013251268), MIC15 (XP_013251270); *Hammondia*
1226 *hammondi*, MIC14, (HHA_218310), MIC15, (HHA_247195); *Neospora caninum*, MIC14 (CEL70510),
1227 MIC15 (CEL70693); *Sarcocystis neurona*, MIC15 (SN3_00200915). **(B)** Schematic representation of
1228 *T. gondii* MIC14 and MIC15 full-length proteins. The numbers identify the amino acid positions of
1229 major domains or elements or the extremes of the protein regions (double arrows) expressed in
1230 bacteria for antibody production. The names of the antibodies are boxed. The numbers of amino
1231 acids and the predicted molecular mass of the full-length proteins are shown in brackets. H-lectin,

1232 H-lectin domain; TSP1, thrombospondin type 1 domain; LP, leader peptide; R1 and R2, N-terminal
1233 repeats; SA, signal-anchor sequence; TM, transmembrane region.
1234
1235 **Fig 3. MIC15 is expressed in *T. gondii* tachyzoites and shows a dispersed intracellular**
1236 **localization. (A)** Western blot analysis of proteins contained in the total tachyzoite lysate (left
1237 panel) or in the excreted-secreted antigens (ESA) fraction and in the corresponding parasite pellet
1238 (P) (right panel). MIC15 was detected with the rabbit antibodies MIC15Nt or MIC15Ct (Fig 2B). The
1239 anti-MIC2 mAb T34A11 was used as positive control of the ESA fraction and its associated pellet.
1240 The intracellular and the cleaved extracellular forms of MIC2 are indicated by white and black
1241 arrowheads, respectively. *T. gondii* GRA1 was used as loading control for the ESA fraction. **(B)**
1242 Immunolocalization of MIC15 in extracellular tachyzoites under non permeabilizing (-Triton X-100)
1243 or permeabilizing (+Triton X-100) conditions. Intact or membrane permeabilized RH parasites were
1244 stained with anti-SAG1 or anti-ROP5 mAbs, respectively, in conjunction with the rabbit serum
1245 MIC15Nt. Scale bar, 5 μm. **(C)** Immunolocalization of MIC15 in intracellular *T. gondii* tachyzoites
1246 with the rabbit serum MIC15Nt. Parasites were double stained with antibodies to protein markers
1247 specific for the micronemes (MIC2), the dense granules (GRA1) or the rhoptries (ROP5). **(D)**
1248 Immunolocalization of MIC15 tagged with the smMYC protein, that consists of 10 copies of the c-
1249 myc epitope inserted into a darkened version of the green fluorescence protein. The punctate
1250 cytoplasmic distribution of tagged MIC15 disclosed by the anti-c-myc mAb is comparable to that of
1251 the native protein shown in (C). Nuclei are stained with DAPI. Scale bar, 5 μm.
1252
1253 **Fig 4. Establishment and validation of a MIC15-iKD conditional-knockdown strain. (A)** Double
1254 homologous recombination strategy used to replace the *MIC15* edogenous promoter with the
1255 Tetracycline Responsive Element (TRE) and the SAG4 minimal promoter. The 5'-terminal exons of

1256 *MIC15* are represented as grey boxes. The arrows represent the primers used for diagnostic
1257 genomic PCR amplifications. **(B)** PCR analysis of the *MIC15-iKD* strain confirming the correct
1258 genomic integration of the DHFR/TRE-SAG4 cassette. **(C)** Time course Western blot analysis of
1259 MIC15-iKD tachyzoites treated with 0.5 μg/ml Atc for 6 to 72 h showing downregulation of MIC15
1260 below detectable level at 29 h. GRA1 was used as loading control. **(D)** Quantitative real-time RT-
1261 PCR analysis of *MIC15* transcription normalized to mRNA levels in strain TATi. Values represent the
1262 means ± SEM of three independent experiments. Statistical significance was determined by the
1263 Student's two tailed t-test. **$p<0.01$. **(E)** Immunofluorescence analysis of intracellular parasites
1264 demonstrating MIC15 depletion in Atc-treated MIC15-iKD tachyzoites. The arrows indicate the
1265 perinuclear accumulation of MIC15 due to protein overexpression in MIC15-iKD strain. Nuclei are
1266 stained with DAPI. Scale bars, 5 μm. **(F)** Plaque assay of the TATi parental strain and MIC15-iKD
1267 mutant grown for 9 days in presence or absence of Atc. The numbers in brackets refer to the initial
1268 inoculum of tachyzoites. **(G)** Western blot analysis showing the rescue of MIC15 expression in
1269 MIC15-iKD parasites complemented with a second copy of the wt gene. **(H)** Plaque assay showing
1270 full restore of the lytic phenotype in complemented MIC15-iKD:wtMIC15 tachyzoites. In all
1271 experiments MIC15 was detected with the rabbit serum MIC15Nt.
1272
1273 **Fig 5. Impact of MIC15 depletion on organelle localization and microneme-dependent functions.**
1274 **(A-D)** Immunolocalization of secretory proteins in MIC15-iKD tachyzoites grown in presence or
1275 absence of Atc for 60 hrs. The parasites were stained with rabbit serum MIC15Nt plus a mAb
1276 specific for either MIC2 (A), MIC8 (B), ROP5 (C) or GRA1 (D). Nuclei are stained with DAPI. Space
1277 bar, 5 μM. **(E)** Western blot analysis of constitutive and ethanol-induced microneme secretion in
1278 MIC15-iKD parasites. The presence of MIC2, MIC4 and MIC8 was revealed in the cytosolic (pellet)
1279 and excreted/secreted antigen (ESA) fractions of TATi and MIC15-iKD tachyzoites grown -/+ Atc for

1280 60 hrs. The uncleaved (intracellular) and processed (extracellular) forms of the microneme
1281 proteins are indicated by arrows or arrowheads, respectively. GRA1 was used as loading control
1282 for the ESA fractions, while cytosolic proteins were normalized with either GRA1 or GAP45. **(F)**
1283 Gliding assay comparing the fraction of motile TATi and MIC15-iKD tachyzoites as revealed by the
1284 presence of $SAG1^{+}$ posterior trails deposited on poly-Lysine-coated glass chamber slides. Prior to
1285 incubation on the substrate for 30 min, the two strains were grown for 60 hrs in presence or
1286 absence of Atc. **(G)** Egress assay estimating the capability of untreated or Atc-treated tachyzoites
1287 of strains TATi and MIC15-iKD to exit the parasitophorous vacuole upon stimulation with the
1288 calcium ionophore A23187. The data in panels F and G are expressed as mean values ± SEM from
1289 three independent experiments conducted in triplicate. In both assays, the Student's two tailed *t*-
1290 test did not reveal statistically significant differences between strains irrespective of MIC15
1291 depletion.
1292
1293 **Fig 6. MIC15 depletion impacts on host cell invasion. (A)** Invasion assay showing a marked
1294 reduction of the number of invaded tachyzoites (red bars) following Atc-induced depletion of
1295 MIC15. The green bars represent the number of attached parasites enumerated for each strain
1296 and condition. Values represent means ± SEM from 4 independent experiments performed in
1297 triplicate. Statistical significance was determined by the Student's two tailed *t*-test. *$p<0.05$,
1298 **$p<0.01$, ***$p<0.001$.
1299
1300 **Fig 7. Selection and characterization of a MIC15-iKD variant strain expressing MIC14. (A)** MIC15-
1301 iKD tachyzoites cultured in presence of Atc for extended periods of time show a partial rescue of
1302 the lytic phenotype. Minuscule plaques detected after 36 days of Atc treatment are indicated by
1303 arrows and a group of them, encircled in white, is shown at higher magnification. Parasites grown

1304 in presence of Atc for 120 days formed larger plaques, still significantly smaller than those
1305 produced omitting Atc from the assay. **(B)** Western blot analysis of strain MIC15-iKD/MIC14^R,
1306 which was cloned from MIC15-iKD parasites propagated in presence of Atc for 120 days. The anti-
1307 MIC14 mouse serum T148 recognized a protein band >198 kDa (arrowhead) in MIC15-iKD/MIC14^R
1308 tachyzoites which was absent in the TATi and MIC15-iKD parental strains. The reactivity of serum
1309 T148 with the >198 kDa product was abolished by the knockout of the *MIC14* gene. **(C)** Schematic
1310 diagram of the strategy used to knockout the *MIC14* gene in the MIC15-iKD/MIC14^R strain. The
1311 promoter region and the first two exons of *MIC14* were replaced with the CAT selectable marker
1312 by double homologous recombination at the sites indicated with dashed lines. Exons in the *MIC14*
1313 gene are shown as purple rectangles with numbers and introns as continuous lines. Primers used
1314 to assess loss of the *MIC14* promoter and 5' terminal exons and integration of the knockout
1315 construct are shown as numbered arrows. **(D)** Analysis of PCR products amplified from the
1316 indicated strains with primers shown in panel C. Migration of size standards in kilobase pairs (Kbp)
1317 are shown to the right. **(E)** Plaque assay demonstrating restoration of the non lytic phenotype
1318 following *MIC14* disruption in MIC15-iKD/MIC14^R tachyzoites. **(F)** Quantitative real-time RT-PCR
1319 analysis of *MIC14* transcription normalized to mRNA levels in the TATi parental strain. Values
1320 represent the means ± SEM of three independent experiments. Statistical analysis was performed
1321 by the Student's two tailed *t*-test.
1322
1323 **Fig 8. Generation and characterization of parasite lines expressing C-terminally tagged MIC14.**
1324 **(A)** The upper part of the diagram shows the single homologous recombination strategy for
1325 integration of the 3x-Ty epitope sequence (in orange) at the 3'end of the *MIC14* coding sequence
1326 in MIC15-iKD/MIC14^R parasites. In the obtained chloramphenicol-resistant strain MIC15-
1327 iKD/MIC14^R-3xTy, the *MIC14* locus was further modified by single homologous recombination

1328 (lower part of the diagram) by replacing the endogenous promoter of *MIC14* with the *T. gondii* α-
1329 tubulin constitutive promoter, obtaining the nourseothricin-resistant strain TUB-MIC14^{R}-3xTy. **(B)**
1330 Western blot analysis of total protein extracts from MIC15-iKD/MIC14^{R} parasites, expressing the
1331 native form of MIC14, and strains MIC15-iKD/MIC14^{R}-3xTy and TUB-MIC14^{R}-3xTy encoding the Ty-
1332 tagged version of the protein. In both tagged strains, the anti-Ty mAb recognized the □250 kDa
1333 full-length MIC14 and two additional bands of approximately 150 and 100 kDa (indicated by
1334 asterisks), likely resulting from specific proteolytic events. As a consequence of promoter
1335 swapping, TUB-MIC14^{R}-3xTy parasites show higher levels of the three MIC14 products. The inner
1336 membrane complex protein GAP45 was used as loading control. **(C)** Immunofluorescence
1337 detection of MIC14-3xTy in strains MIC15-iKD/MIC14^{R}-3xTy and TUB-MIC14^{R}-3xTy. The two tagged
1338 strains and the parental line MIC15-iKD/MIC14^{R} were dual stained with an anti-Ty mAb and the
1339 anti-MIC15 serum MIC15Nt. Nuclei are stained with DAPI. Scale bars, 5 μm.
1340
1341 **Fig 9. MIC15 and MIC14 are novel components of the rhoptry discharge pathway.** Rhoptry
1342 secretion assay based on the detection of ROP1^{+} evacuoles released in the host cell by
1343 Cytochalasin D-arrested extracellular tachyzoites. Values represent the percentage of evacuole-
1344 associated tachyzoites and are expressed as means ± SEM from three independent experiments
1345 performed in triplicate. Statistical significance was determined by the Student's two tailed *t*-test.
1346 *$p<0.05$, **$p<0.01$. The number of parasites able to produce evacuoles was significantly lower in
1347 MIC15-depleted tachyzoites (red bars) compared to the untreated MIC15-iKD control and the
1348 parental strain. No statistically significant reduction in evacuole formation was observed in MIC15-
1349 iKD/MIC14^{R} parasites depleted of MIC15 (green bars), demonstrating that MIC14 upregulation is
1350 able to functionally compensate the MIC15-dependent rhoptry secretion defect. The strain RON5-
1351 iKD defective in rhoptry secretion was used as positive control (grey bars). Based on this evidence,

1352 MIC15 and MIC14 are renamed rhoptry discharge factor 1 (RDF1) and rhoptry discharge factor 2

1353 (RDF2), respectively.

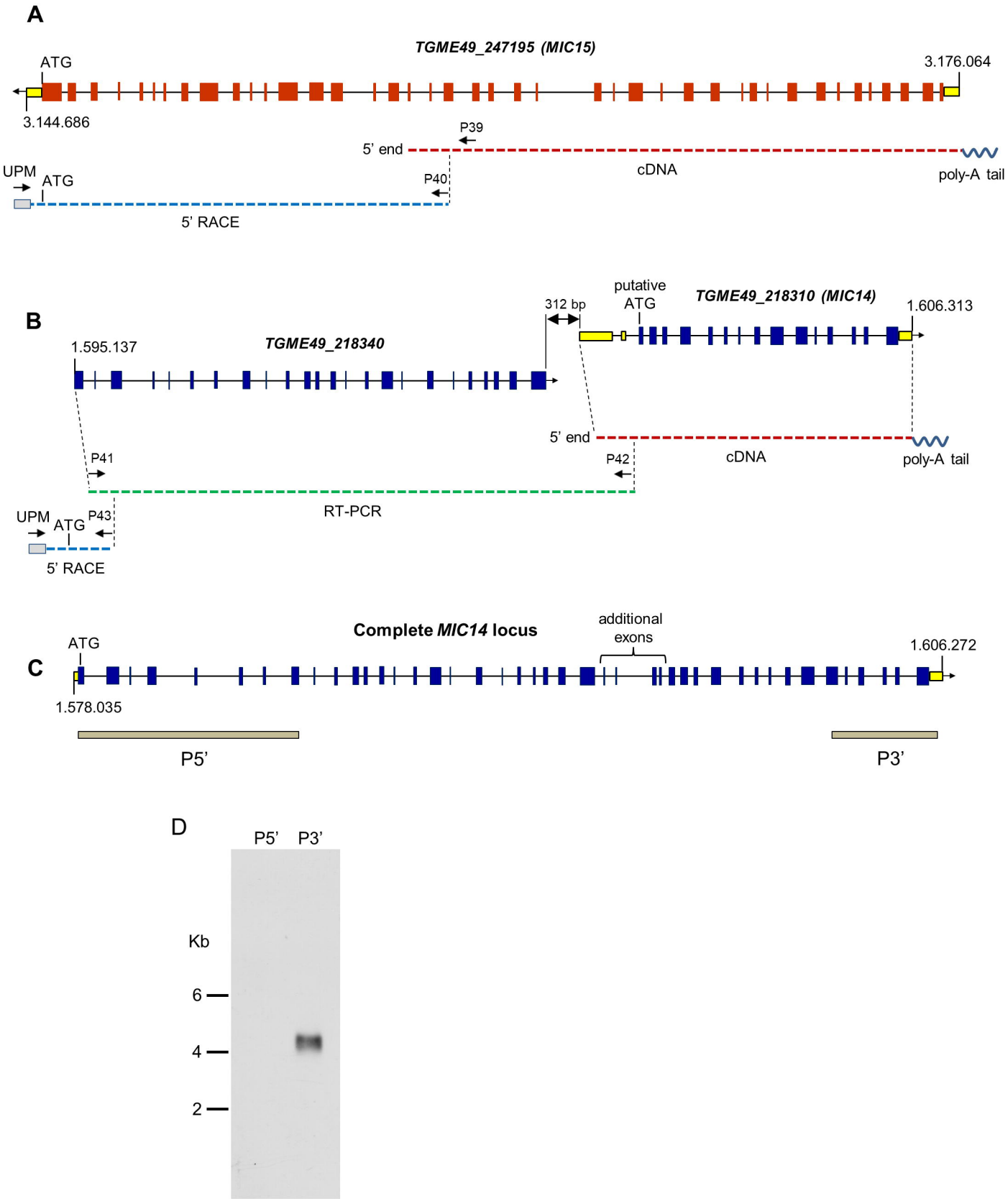
A
TGME49_247195 (MIC15)
ATG
3.176.064
3.144.686
P39
5' end
cDNA
poly-A tail
UPM
ATG
P40
5' RACE
B
putative
ATG
TGME49_218310 (MIC14)
312 bp
1.606.313
1.595.137
TGME49_218340
5' end
cDNA
poly-A tail
P41
P42
RT-PCR
UPM
ATG
P43
5' RACE
C
Complete MIC14 locus
additional
exons
ATG
1.606.272
1.578.035
P5'
P3'
D
P5'
P3'
Kb
6
4
2

Figure 1

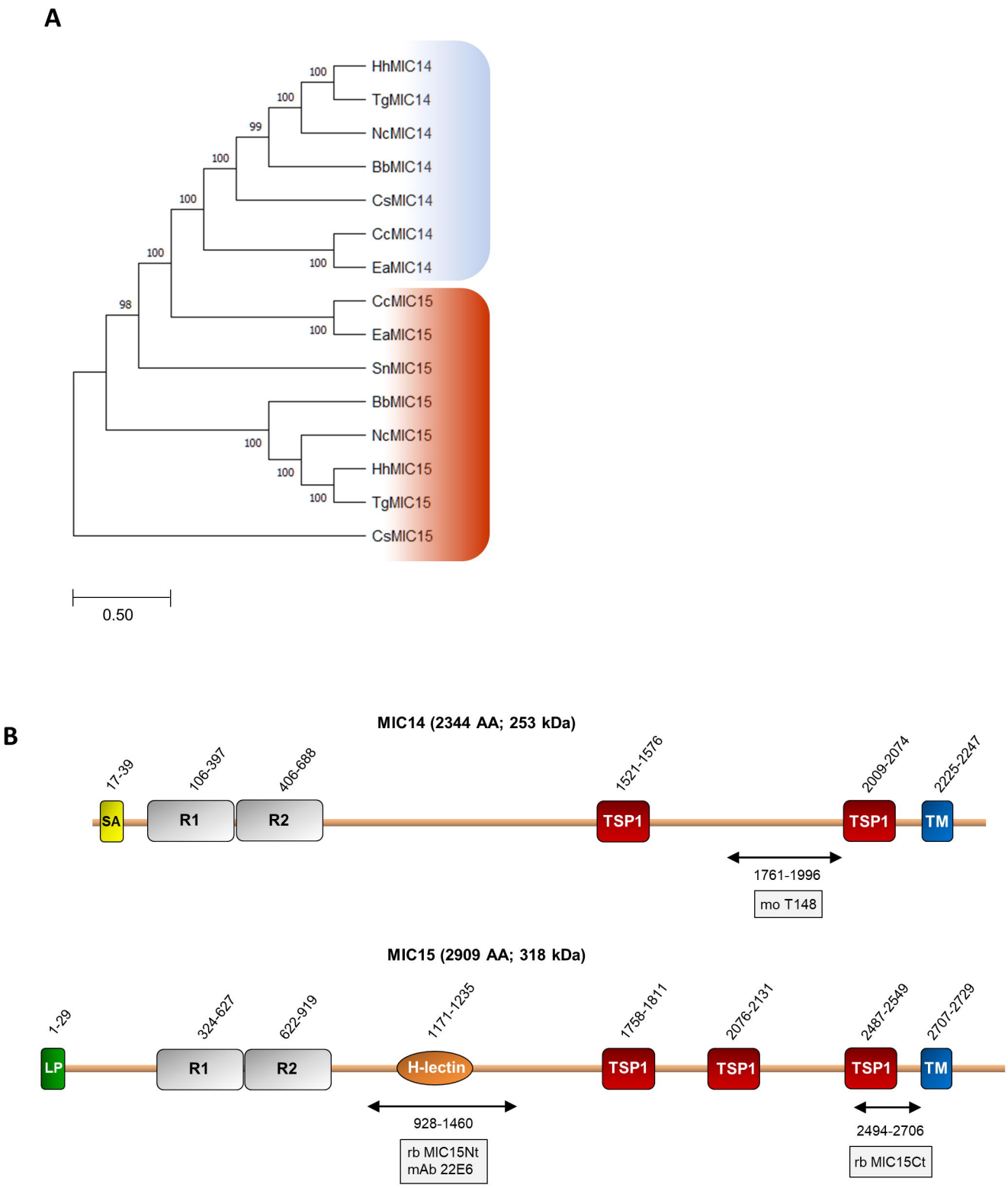
A
HhMIC14
TgMIC14
NcMIC14
BbMIC14
CsMIC14
CcMIC14
EaMIC14
CcMIC15
EaMIC15
SnMIC15
BbMIC15
NcMIC15
HhMIC15
TgMIC15
CsMIC15
100
100
99
100
100
100
100
98
100
100
100
100
0.50
B
MIC14 (2344 AA; 253 kDa)
17-39
106-397
406-688
1521-1576
2009-2074
2225-2247
SA
R1
R2
TSP1
TSP1
TM
1761-1996
mo T148
MIC15 (2909 AA; 318 kDa)
1-29
324-627
622-919
1171-1235
1758-1811
2076-2131
2487-2549
2707-2729
LP
R1
R2
H-lectin
TSP1
TSP1
TSP1
TM
928-1460
rb MIC15Nt
mAb 22E6
2494-2706
rb MIC15Ct

Figure 2

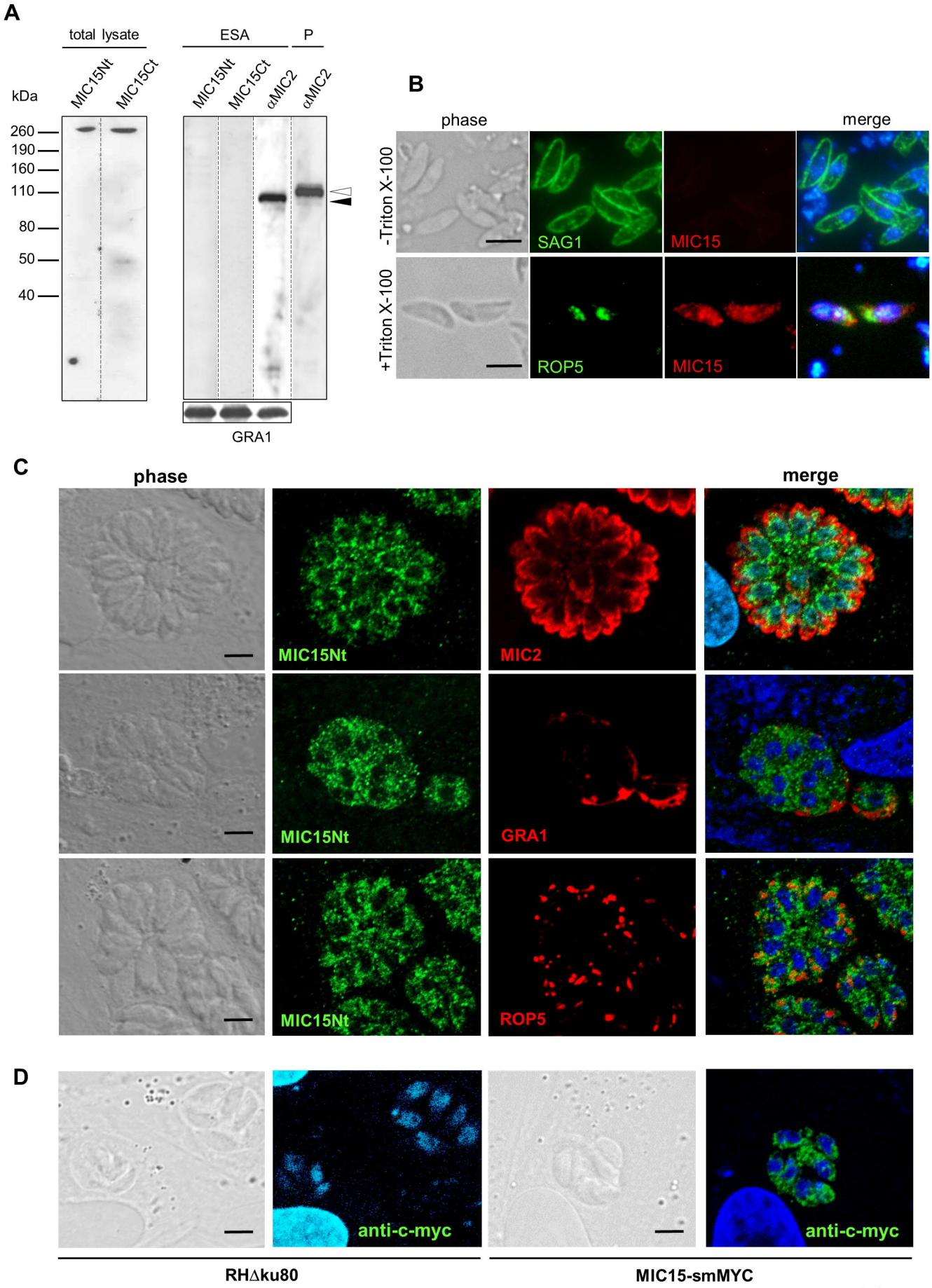
A
total lysate
ESA
P
kDa
MIC15Nt
MIC15Ct
MIC15Nt
MIC15Ct
αMIC2
αMIC2
260
190
160
110
80
50
40
GRA1
B
phase
merge
-Triton X-100
+Triton X-100
SAG1
MIC15
ROP5
MIC15
C
phase
merge
MIC15Nt
MIC2
MIC15Nt
GRA1
MIC15Nt
ROP5
D
anti-c-myc
anti-c-myc
RHΔku80
MIC15-smMYC

Figure 3

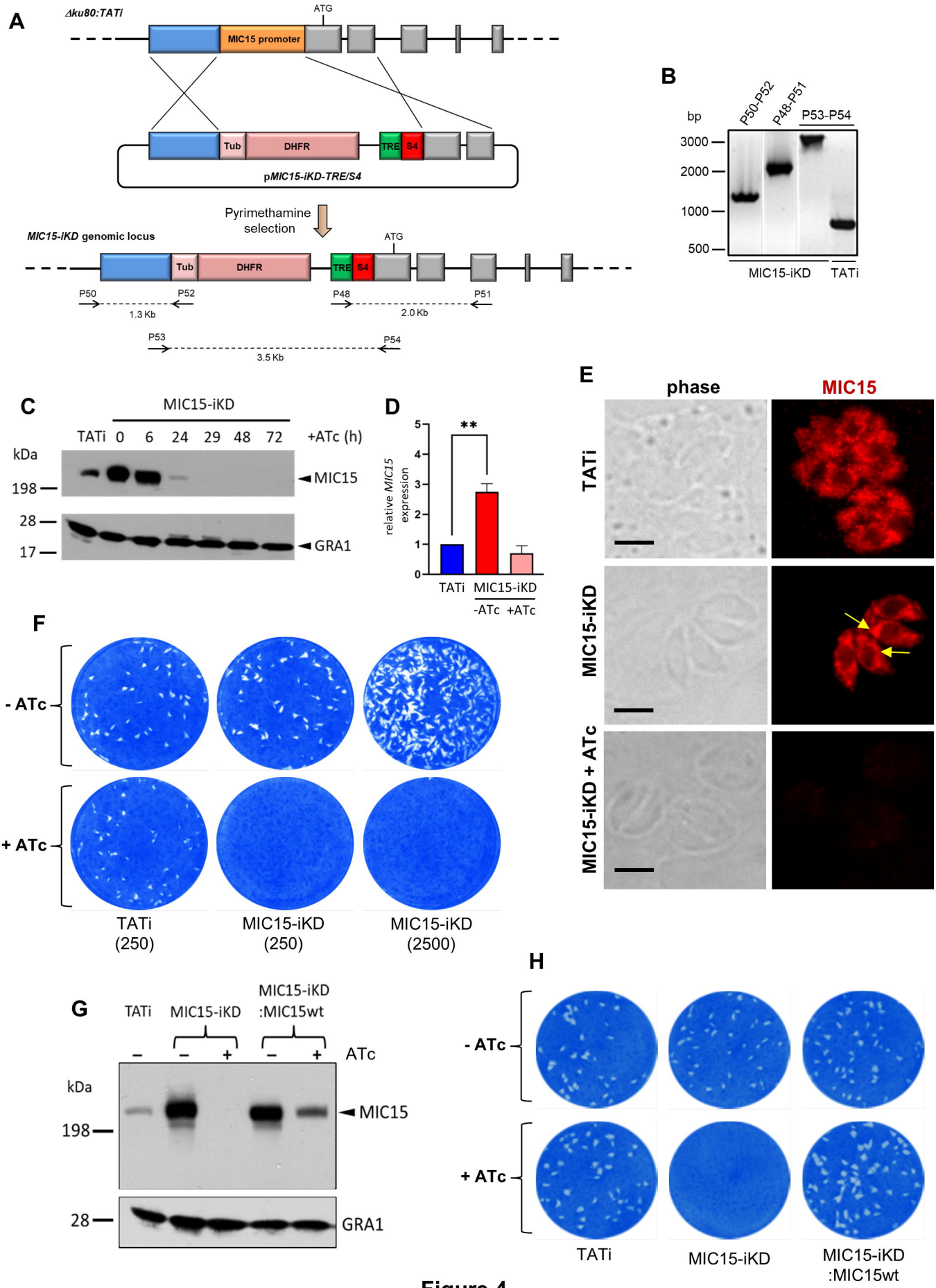
A
Δku80:TATi
ATG
MIC15 promoter
Tub
DHFR
TRE
S4
pMIC15-iKD-TRE/S4
Pyrimethamine selection
MIC15-iKD genomic locus
P50
P52
1.3 Kb
P48
P51
2.0 Kb
P53
P54
3.5 Kb
B
bp
P50-P52
P48-P51
P53-P54
3000
2000
1000
500
MIC15-iKD
TATi
C
MIC15-iKD
TATi 0 6 24 29 48 72 +ATc (h)
kDa
198
28
17
MIC15
GRA1
D
relative MIC15 expression
**
TATi
MIC15-iKD
-ATc +ATc
E
phase
MIC15
TATi
MIC15-iKD
MIC15-iKD + ATc
F
- ATc
+ ATc
TATi (250)
MIC15-iKD (250)
MIC15-iKD (2500)
G
TATi
MIC15-iKD
MIC15-iKD :MIC15wt
ATc
kDa
198
28
MIC15
GRA1
H
- ATc
+ ATc
TATi
MIC15-iKD
MIC15-iKD :MIC15wt

Figure 4

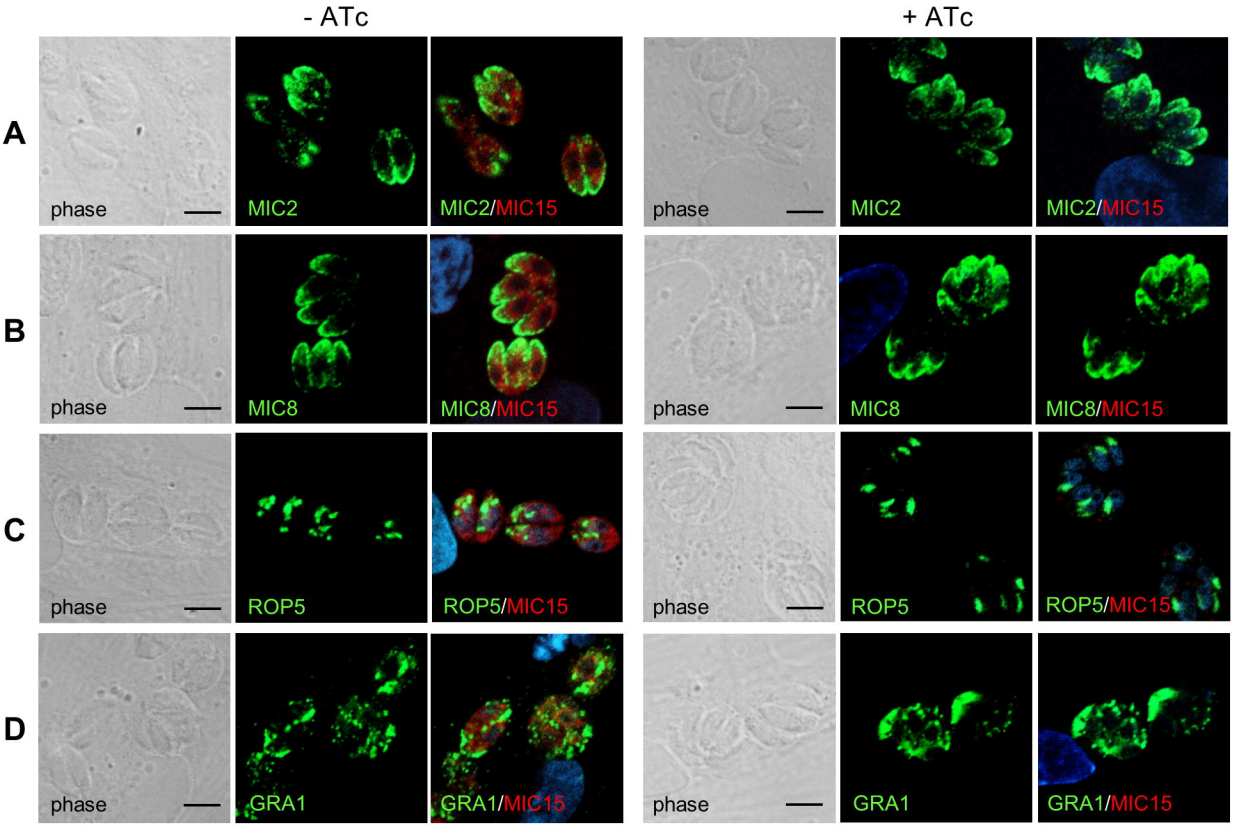
- ATc
+ ATc
A
B
C
D
phase
MIC2
MIC2/MIC15
MIC8
MIC8/MIC15
ROP5
ROP5/MIC15
GRA1
GRA1/MIC15

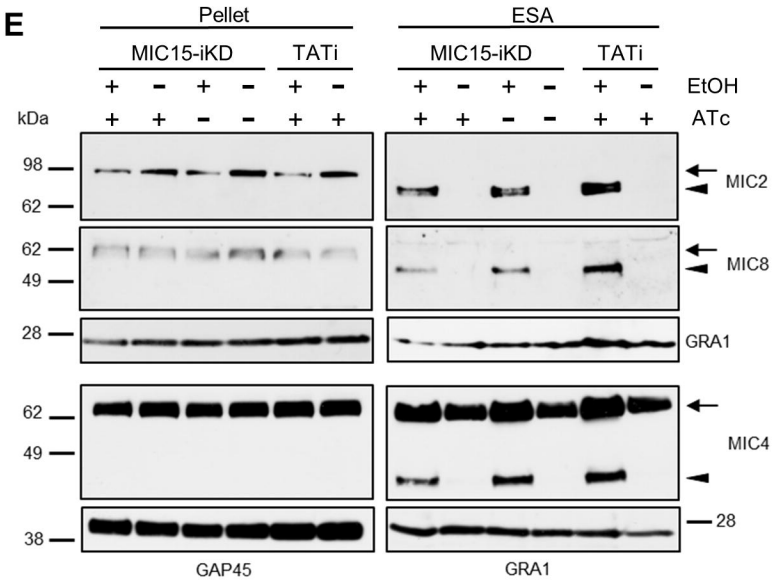
E
Pellet
ESA
MIC15-iKD
TATi
EtOH
ATc
kDa
98
62
49
28
38
MIC2
MIC8
GRA1
MIC4
GAP45

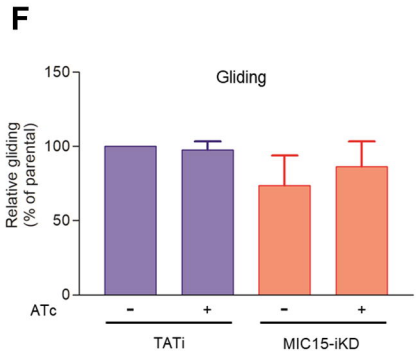
F
Gliding
Relative gliding (% of parental)
150
100
50
0
ATc
TATi
MIC15-iKD

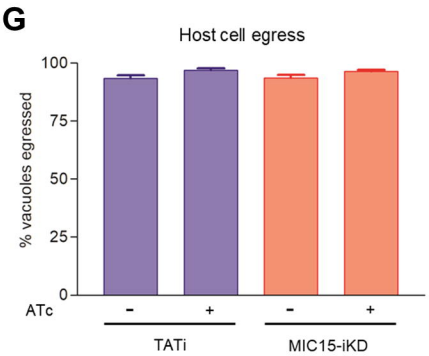
G
Host cell egress
% vacuoles egressed
100
75
50
25
0
ATc
TATi
MIC15-iKD

Figure 5

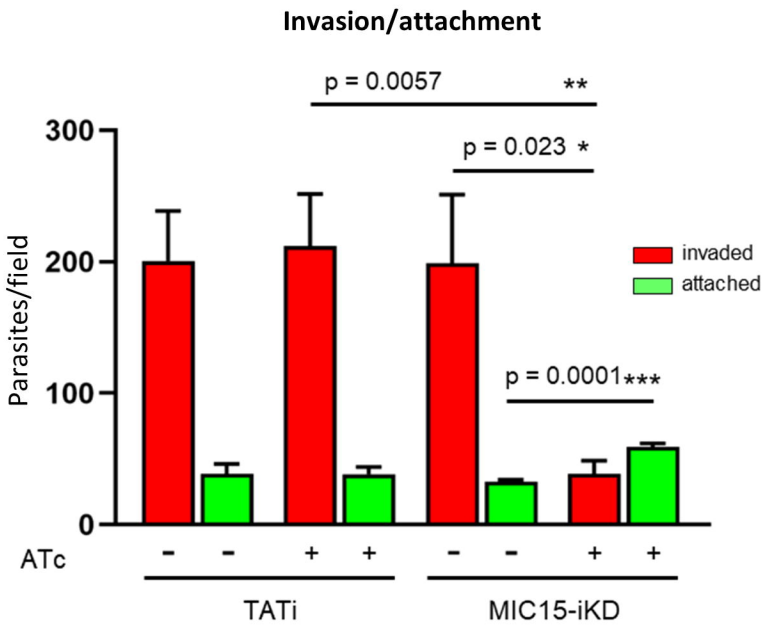
Invasion/attachment
p = 0.0057 **
p = 0.023 *
p = 0.0001***
300
200
100
0
Parasites/field
invaded
attached
ATc
- - + + - - + +
TATi
MIC15-iKD

Figure 6

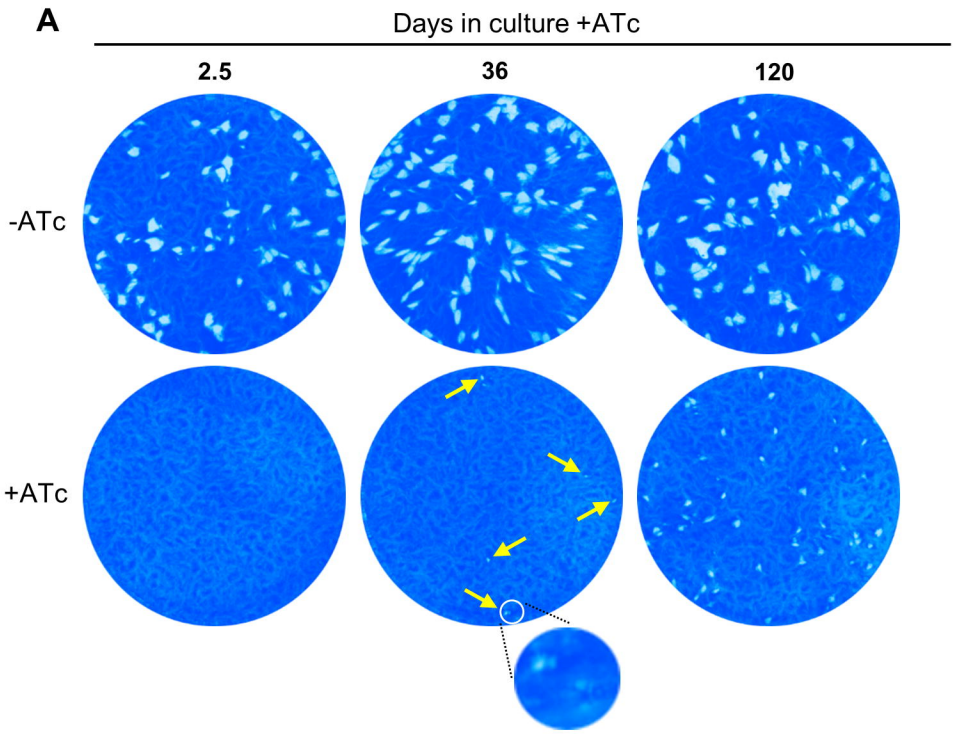
A
Days in culture +ATc
2.5
36
120
-ATc
+ATc

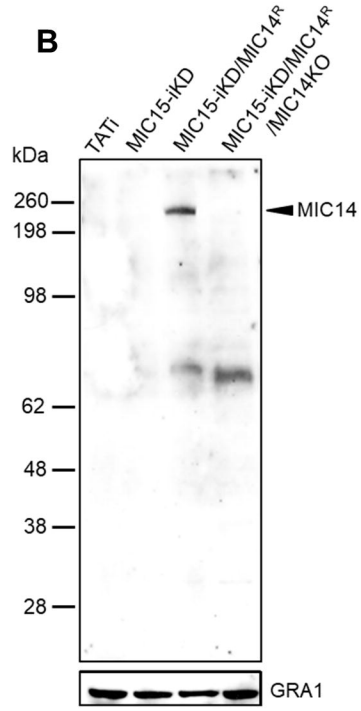
B
TATi
MIC15-iKD
MIC15-iKD/MIC14R
MIC15-iKD/MIC14R /MIC14KO
kDa
260
198
98
62
48
38
28
MIC14
GRA1

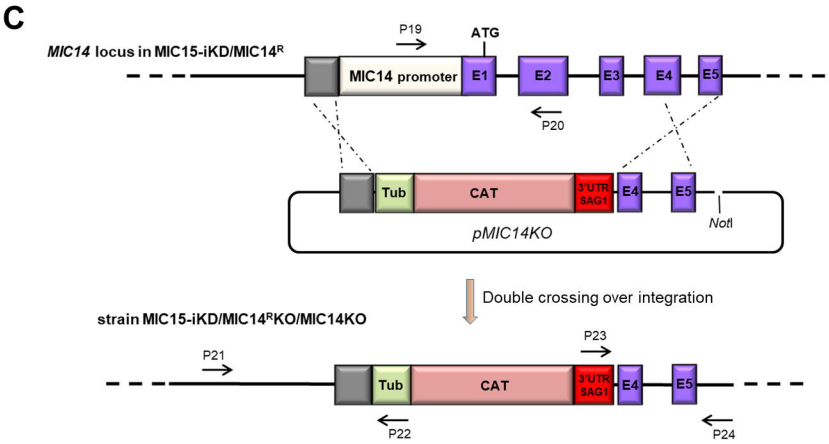
C
MIC14 locus in MIC15-iKD/MIC14R
P19
ATG
MIC14 promoter
E1
E2
E3
E4
E5
P20
Tub
CAT
3'UTR SAG1
pMIC14KO
NotI
Double crossing over integration
strain MIC15-iKD/MIC14RKO/MIC14KO
P21
P23
P22
P24

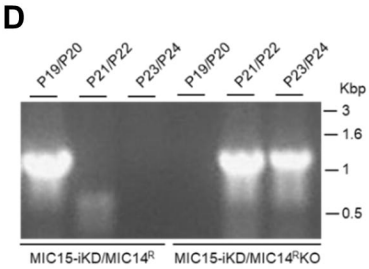
D
P19/P20
P21/P22
P23/P24
P19/P20
P21/P22
P23/P24
Kbp
3
1.6
1
0.5
MIC15-iKD/MIC14R
MIC15-iKD/MIC14RKO

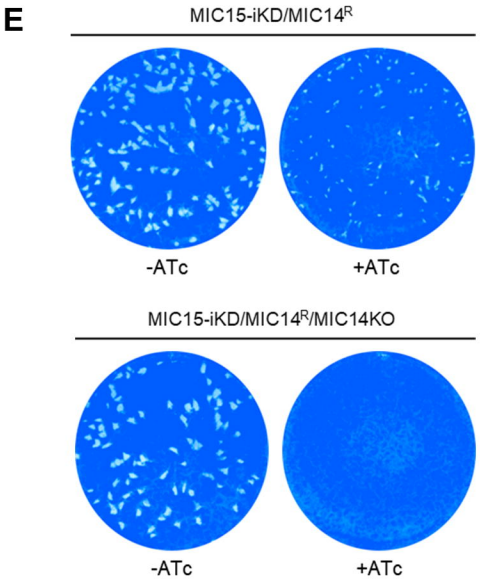
E
MIC15-iKD/MIC14R
-ATc
+ATc
MIC15-iKD/MIC14R/MIC14KO
-ATc
+ATc

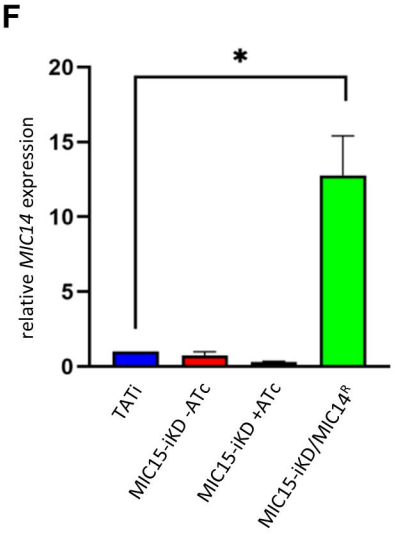
F
*
20
15
10
5
0
relative MIC14 expression
TATi
MIC15-iKD -ATc
MIC15-iKD +ATc
MIC15-iKD/MIC14R

Figure 7

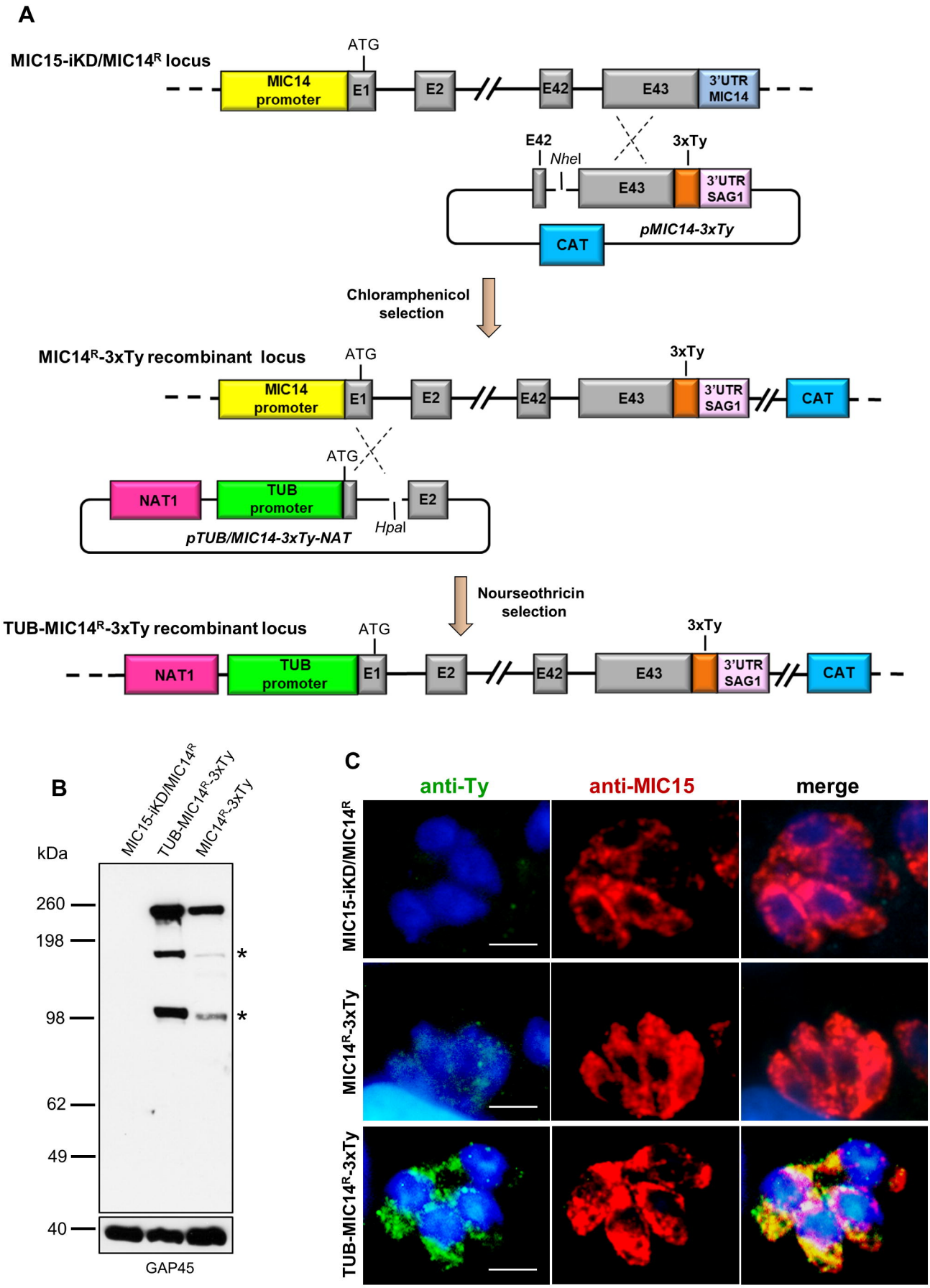
A
MIC15-iKD/MIC14R locus
ATG
MIC14 promoter
E1
E2
E42
E43
3'UTR MIC14
E42
NheI
3xTy
E43
3'UTR SAG1
CAT
pMIC14-3xTy
Chloramphenicol selection
MIC14R-3xTy recombinant locus
ATG
3xTy
MIC14 promoter
E1
E2
E42
E43
3'UTR SAG1
CAT
ATG
NAT1
TUB promoter
E2
HpaI
pTUB/MIC14-3xTy-NAT
Nourseothricin selection
TUB-MIC14R-3xTy recombinant locus
ATG
3xTy
NAT1
TUB promoter
E1
E2
E42
E43
3'UTR SAG1
CAT
B
MIC15-iKD/MIC14R
TUB-MIC14R-3xTy
MIC14R-3xTy
kDa
260
198
98
62
49
40
*
*
GAP45
C
anti-Ty
anti-MIC15
merge
MIC15-iKD/MIC14R
MIC14R-3xTy
TUB-MIC14R-3xTy

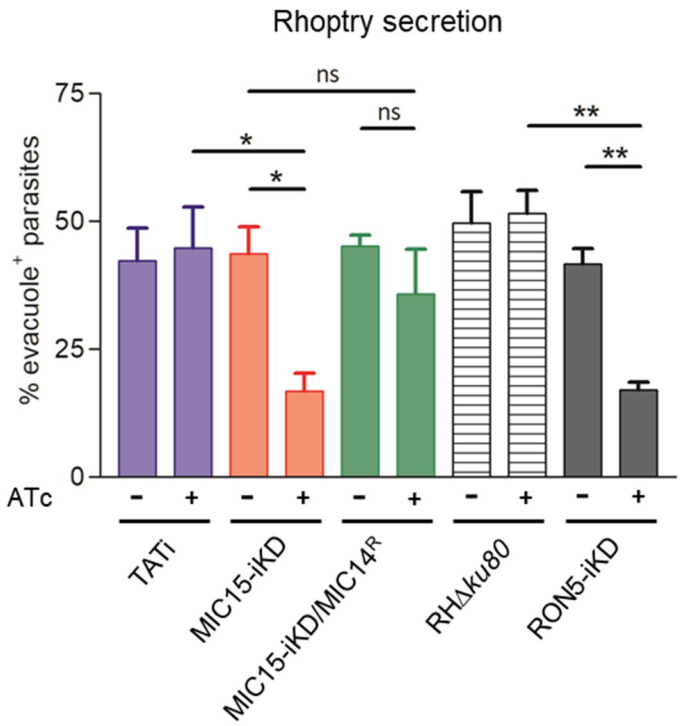
Rhoptry secretion
% evacuole+ parasites
75
50
25
0
ns
ns
*
*
**
**
ATc
-
+
-
+
-
+
-
+
-
+
TATi
MIC15-iKD
MIC15-iKD/MIC14R
RHΔku80
RON5-iKD

Figure 9